R. & M. No. 3041
(18,246)
A.R.C. Technical Report

MINISTRY OF SUPPLY

AERONAUTICAL RESEARCH COUNCIL
REPORTS AND MEMORANDA

The Icing of Compressor Blades and their Protection by Surface Heating

By

G. L. SHIRES and G. E. MUNNS

LONDON: HER MAJESTY'S STATIONERY OFFICE
1958
PRICE 15s. 0d. NET

The Icing of Compressor Blades and their Protection by Surface Heating

By

G. L. SHIRES and G. E. MUNNS

COMMUNICATED BY THE DIRECTOR GENERAL OF SCIENTIFIC RESEARCH (AIR)

MINISTRY OF SUPPLY

*Reports and Memoranda No. 3041**

June, 1955

Summary.—This paper describes an investigation into the feasibility of protecting compressor blades against ice accretion by the method of surface heating.

Experiments with surface-heated inlet guide vanes and stator blades were performed in the icing tunnel at the Royal Aircraft Establishment. An electrically heated blade, having almost uniform surface temperature, was developed and then used to determine the effects of air velocity and icing conditions on the minimum heat flow required to prevent the formation of ice. The theoretical method, by J. K. Hardy, of calculating this heat requirement shows reasonable agreement with the experimental results.

Steel, copper and copper-plated gas-heated blades with various internal passage shapes were also tested and their heat requirement compared with those of the corresponding electrically heated blades under the same external conditions. The ratio of the latter to the former heat quantity is called the thermal efficiency and is shown to be a function of internal passage shape, blade material, conductivity and dimensions, the gas flow and the external conditions.

Finally, a method of estimating the pressure drop through the gas-heated blades is suggested and a worked example is included to demonstrate the method of assessing the mass flow and pressure required to anti-ice a row of inlet guide vanes by means of a compressor bleed.

1. *Introduction.*—The icing of aircraft in flight is caused by the impact and freezing of supercooled water droplets on forward facing parts of the aircraft. Such droplets occur in certain cloud formations at low ambient temperatures.

The axial-flow compressor of a gas turbine has been found to be particularly susceptible to ice accretion. Experience, both in flight and on the test-bed, has shown that ice forms on the intake surfaces, the bullet, spider, inlet guide vanes and, to a lesser extent, the first stator row. Without protection for these surfaces, icing may cause a reduction of inlet area with attendant reductions of air mass flow and power, and increase of turbine temperature or, at the worst, pieces of ice breaking away from upstream surfaces may damage or cause complete failure of the compressor.

Methods of preventing the formation of ice on gas-turbine engines include charge heating, where the whole of the aspired air is heated; melting-point depressants, which are usually one or other of the alcohol group; inertia separation of the water particles, and surface heating. At present, surface heating appears to be the most desirable method because of the relatively small amounts of heat required. The investigation described in this report, which deals only with inlet guide vanes and stator blades, is part of a larger programme of research covering all the susceptible surfaces previously mentioned.

The experiments were performed in the icing tunnel at the Royal Aircraft Establishment where icing conditions likely to be met in flight could be simulated. The test blades, arranged in cascades representing typical stator and inlet-guide-vane configurations, were heated either electrically or by hot gas. Both methods of protection depended upon keeping the minimum

* N.G.T.E. Report R.178, received 24th February, 1956.

surface temperature above 0 deg C. The heat quantity required to maintain an electrically heated copper blade ice-free was taken as a basis for comparing the performance of various gas-heated blades under the same external conditions.

The aims of the investigation were:

(*a*) to determine the effect of air temperature, liquid-water concentration, droplet size and air velocity on the minimum heat quantity necessary for anti-icing;

(*b*) to determine and compare the efficiencies of various types of gas-heated blades and to find a relationship between these efficiencies, the internal passage shape, the conductivity of the blade material, the blade dimensions, the gas mass flow and the external conditions.

2. *The Apparatus.*—The test blade in each experiment was mounted in the centre of a cascade attached to the outlet of the R.A.E. icing tunnel. One cascade represented a row of stator blades and the other, a row of inlet guide vanes. The air of the tunnel was cooled by passing over tubes carrying a brine solution at about — 30 deg C. Water jets well upstream of the cascade provided the equivalent of the cloud water content, the drops being supercooled on reaching the cascades.

2.1. *The Icing Tunnel.*—The main features of the tunnel, apart from the cooling system, are shown in Fig. 1.

A maximum air velocity, V_1, of 500 ft/sec was obtainable upstream of the cascade at a minimum total air temperature, t_{tot}, of — 29 deg C. Temperature and velocity could be varied by allowing air to bypass the cooler and by altering the input to the fan motor.

During icing tests, water was introduced through four jets of the type shown inset in Fig. 1. Water passes through the central hole while air expands through the surrounding annulus, breaking up the water column into very small droplets. The mean size of the water droplets was found to be a function of the water flow and the air pressure. The jets were calibrated on this basis using the oiled-slide technique developed by the R.A.E. In this method a sample is caught on a coated slide held in the working section, and the mass mean droplet size assessed by measuring, under a microscope, the diameters of the droplets caught.

The mean water concentration just upstream of the cascade was calculated in each case from the measured value of the water flow, G_{wj}, to the jets, the air velocity V_1, and the tunnel cross-sectional area at this point. The amount of water caught on the tunnel walls was assumed to be negligible compared with the total rate of flow. The position of the jets was arranged to give uniform distribution with a tunnel end similar to the ones used in the tests; the uniform thickness of the deposit over the length of the unheated blade shown in Fig. 3 is evidence of this. Since, during the tests, the water was sprayed into a pre-cooled air stream its temperature at entry had to be kept well above 0 deg C to prevent it freezing in the jets. The actual temperature of the droplets on reaching the blades was, therefore, unknown and extremely difficult to measure. However, it can be calculated, and in Appendix I this is done using a theory developed by J. K. Hardy[1]. The results suggest that the droplet temperature on reaching the blade was close to the effective air temperature, t_1'.

2.2. *The Cascades.*—Two cascades were used, each consisting of a removable test blade and seven gas-heated dummy blades all of the form 10C4/25/P40 and having the following dimensions:

Chord	c	$= 1{\cdot}3$ in.
Length in air stream	L	$= 3{\cdot}0$ in.
Pitch	s	$= 0{\cdot}975$ in.
External surface area	S_a	$= 8{\cdot}12$ in.^{2}.

The difference in the two cascades was in the stagger angle alone.

The values were:

(*a*) for the stator cascade .. .. .. $\xi = -37{\cdot}6$ deg

(*b*) for the I.G.V. cascade .. .. .. $\xi = +17{\cdot}4$ deg.

The air inlet angle to the stator cascade was varied by the substitution of different tunnel ends. The values of incidence obtained for the stator cascade were + 10 deg, 0 deg and − 10 deg, whereas the incidence to the inlet-guide-vane cascade was maintained at 0 deg throughout the tests.

2.3. *Tunnel Instrumentation.*—During each test measurements were made of air temperature and velocity in the tunnel.

The effective air temperature, t_1', just before the accelertaing section (*see* Fig. 1), was measured by means of a mercury-in-glass thermometer which was removed when the water was turned on, as icing of the instrument would otherwise have occurred. As the velocity at this point did not exceed 50 ft/sec, the difference between this temperature and the total temperature, t_{tot}, was always less than 0·2 deg C and was, therefore, neglected. Readings were taken before and after each test and the mean values used in the analysis.

To obtain a uniform velocity profile, boundary-layer suction was employed at the tunnel end. Several static-pressure tappings were drilled in the vertical walls of each tunnel end near to the cascade and the suction adjusted to give a uniform pressure distribution. These tappings were also used in conjunction with the total pressure, p_{tot}, measured by a pitot tube upstream of the water jets to give a reading of dynamic head and hence of the velocity, V_1, just upstream of the cascade. This system of velocity measurement, which operated during icing, was used in conjunction with a direct check measurement of the downstream velocity, V_2, with a standard air-speed indicator.

3. *Icing Conditions.*—The term ' icing conditions ' denotes the state of the atmosphere; in the engine it refers to the atmosphere into which the aircraft is flying; in the wind tunnel to the air upstream of the cascade. It is defined by the values of the air temperature, the liquid-water concentration and the droplet size.

In both the engine and the wind tunnel the degree of severity of the ice accretion depends upon the icing conditions and it is useful to compare the likely range of values in the two cases. Since the gas-turbine engine is apparently susceptible to short periods of icing, the severest condition, even though of minor extent, must be considered. According to a paper by Jones and Lewis[2] the maximum instantaneous ' conditions ' may be summarised as in Table I.

In comparison, the range of icing conditions obtained in the icing tunnel was as follows:

Air temperature, t_{tot}, = 0 to − 20 deg C

Water concentration, n, = 0 to 6·5 gm/m^3

Droplet size, d, = 15 to 50 microns.

The experiments, therefore, covered a range of icing conditions of the same order as that likely to be met in normal flight, with the exception of the low-temperature case.

4. *Icing of Unheated Blades.*—When a cascade of blades or a single blade is exposed to a sub-zero air stream containing supercooled water droplets, a film of ice immediately forms and in a short period of time grows to an appreciable thickness. The shape and thickness of the resulting ice deposit depends upon the blade shape, its orientation relative to the air stream, the air velocity and the icing conditions; so, also, does the associated pressure loss and reduction in mass flow through the cascade. To determine the effect of some of these parameters a series of tests was made with unheated blades, both isolated and in cascade.

4.1. *The Mechanism of Icing.*—The ice formation on an unheated stator blade in cascade at zero incidence is shown in Fig. 3, looking towards the concave surface from downstream. For clearness all but the test blades were maintained at a temperature above 0 deg C during the run and were not, therefore, subject to ice accretion. As is shown, the ice formed uniformly over the concave surface and reached a thickness of approximately $\frac{1}{8}$ in. in 60 sec. At the leading edge, not visible on the photograph, the deposit was thickest, while on the convex surface only a thin film adhered. The type of ice, under the conditions of the test, was what has been described[3] as rime ice, the crystalline formation being clearly visible. The ice was extremely tenacious. Scraping removed the top crystals but left a hard, thin layer of ice attached to the surface.

To obtain a clearer picture of the ice formations all over the blade an extension holding a single blade was attached to the tunnel end. This feature is shown in Fig. 4, where the direction from which the photographs were taken is indicated. A comparison of the ice build-up on this blade under different conditions can be obtained from Fig. 5, which contains a series of photographs taken after 120 seconds of continuous ' icing '. In Figs. 5a and 5b, both taken with an air temperature, t_1', of $-2{\cdot}5$ deg C, the ice is transparent and comes under the category of glaze ice, in Figs. 5c and 5d, where $t_1' = -12$ deg C, glaze ice remains only at the nose; and in Figs. 5e and 5f at $t_1' = -29$ deg C most of the ice exhibits the crystalline structure of rime.

The formation of the two different kinds of ice is clearly due to temperature differences. The transparent appearance of glaze ice indicates that at one stage there is water in the liquid state upon the blade surface and that locally the temperature is, for a time at least, above 0 deg C. Now glaze ice appears quite plainly when the air temperature is as low as $-2{\cdot}5$ deg C and when the water is supercooled to at least $-2{\cdot}0$ deg C. The source of heat which raises the water temperature to 0 deg C must, therefore, be the latent heat of fusion which is liberated when some of the droplets freeze on impact.

At present the mechanism of icing is not properly understood and it is not clear what happens to the supercooled droplets immediately after impact. Whether the whole or only part of each droplet changes to ice and at what temperature the ice forms are questions that could only be answered with confidence after a more detailed investigation. It is possible, however, to consider the overall heat balance without knowledge of the intermediate stages, for eventually the latent heat liberated must be dissipated either by convection and evaporation to the air stream or by conduction to the surrounding ice or to the blade.

Let us consider the heat balance for the blade shown in Fig. 5.

If G_w is the rate of water catch, x per cent of which is turned to ice, and L_f is the latent heat of fusion of ice, the heat liberated during the change of state is:

$$H = xG_wL_f. \qquad (1)$$

Some of this heat is dissipated by convection and evaporation to the air stream and the remainder is used in raising the temperature of the water from its initial value, t_w, to the blade temperature, t_b. Hence, in thermal equilibrium the equation for steady heat flow is:

$$xG_wL_f = G_wc_{p\,w}(t_b - t_w) + h_m(1 + X)S_a(t_b - t_1'), \qquad (2)$$

where h_m and S_a are the mean heat-transfer coefficient and the total surface area of the ice-coated blade respectively, and X is the ratio of evaporative to convective heat transfer. Now in the case considered $c_{p\,w} = 1{\cdot}0$ and $t_w \simeq t_1'$, so that:

$$xG_wL_f = [G_w + h_m(1 + X)S_a]\,(t_b - t_1'). \qquad (3)$$

When no glaze is present all of the water reaching the blade is turned to ice and $x = 1{\cdot}0$. Then:

$$t_b - t_1' = \frac{G_wL_f}{G_w + h_m(1 + X)S_a}. \qquad (4)$$

The blade temperature in this case is, therefore, higher than the air temperature by an amount depending upon the rate of water catch and the heat-transfer coefficient. Assuming a value of $h_m S_a$ equal to 1·5 times that for the blade without ice and a water catch corresponding to the projected area, and substituting these values in this equation we get (Appendix II):

$$t_b - t_1' \simeq 9{\cdot}2 \text{ deg C} . \qquad (5)$$

At air temperatures less than — 9·2 deg C, therefore, one would expect the ice to be entirely rime.

It is evident from the photographs in Fig. 5 that the change from rime ice to glaze ice occurs at a value of t_1' near — 12 deg C, which suggests that the explanation offered is reasonable. For air temperatures above this initial value the blade temperature would be close to 0 deg C, and part of the water catch would either remain in, or return to, the liquid state and subsequently be blown off into the air stream. From equation (3), the fraction of impinging water remaining as ice is given by:

$$x = \frac{[G_w + h_m(1 + X)S_a](0 - t_1')}{G_w L_f} \simeq \frac{(0 - t_1')}{9{\cdot}2} .$$

On this basis the percentage of water converted to ice when $t_1' = -2{\cdot}5$ deg C would be approximately 27 per cent.

Another noticeable difference in ice formation is that between Figs. 5e and 5f. In the former, which represents a blade subject to the impingement of droplets of 28 microns diameter, the line of crystal growth is at approximately 45 deg to the blade surface, while in the latter with droplets of 15 microns diameter, the angle of growth is much more acute. This difference, which is shown diagrammatically in Fig. 4, is also evident to a lesser extent between Figs. 5c and 5d. The reason for this phenomenon is not clear, although rate of crystallization of the droplets probably plays a part.

4.2. *Effects of Ice Accretion.*—The growth of ice on compressor blades in cascades affects their performance adversely in two ways. It spoils the smooth aerofoil shape and thus reduces the pressure rise in the stage, while at the same time it reduces the mass flow by blocking the air passages. Both of these effects were evident when the whole of the cascade was allowed to ice up.

The performance of this stator cascade is illustrated graphically in Figs. 6 and 7 as a function of time. The first graph shows the mass flow plotted as a percentage of the mass flow in an ice-free cascade, and the second shows the pressure drop as a percentage of the dynamic head at inlet to the cascade. Of the factors governing ice accretion, water concentration and air temperature are clearly the most important.

For an air velocity of 350 ft/sec, a temperature of — 16 deg C, and a water concentration of 1·5 gm./m^3, the mass flow was reduced by 20 per cent in 45 sec and in the same period the pressure rise was completely eliminated. When the air temperature was — 5 deg C the time to reach this state was doubled. Under all conditions the deterioration of performance was initially very rapid.

Over longer periods the pressure loss continued to increase rapidly but the rate of mass-flow reduction became less, probably because of the progressively smaller quantities of water carried into the cascade. The blocking of the air passage took place chiefly at the leading edge where the build up of ice was greatest. Under certain conditions caps similar to that shown in Fig. 5e were formed and appeared to block a large part of the air passage. As all these tests were made with 20-micron-diameter particles, the results obtained with the isolated blade, Figs. 5e and 5f, suggest that smaller particle sizes would have produced a smoother ice deposit and, therefore, a less rapid rate of blockage.

5. *Anti-Icing by Electrical Heating.*—In the part of the investigation concerned with the effect of air velocity and icing conditions, electrically heated blades were used. The temperature distribution over the surface of each of these blades, with a voltage applied and ice just forming at the trailing edge, was nearly uniform and very little heat was wasted in local overheating. For this reason the heating efficiency was approximately 100 per cent, and the heat quantity required, which was therefore a minimum, was taken as a datum and its variation with external conditions investigated.

5.1. *The Electrically Heated Blades.*—The blades were made of solid copper with six lengthwise holes of diameter 0·060 in. as shown in Fig. 8. The best temperature distribution was obtained when single-wire heating elements were placed in four of the holes leaving the central two unheated. One of these central holes was used to house a thermocouple lead, the couple junction being soldered into the blade surface and then made flush. It was estimated that the total surface temperature variation with this arrangement was less than 2·5 deg C with ice just beginning to form.

5.2. *The Critical Heat Quantity.*—The procedure for determining the critical heat quantity, *i.e.*, the minimum heat input necessary to keep the blade free from ice, was as follows:

First the air velocity and temperature in the wind tunnel were set at the values decided upon for the test. The required water content was then introduced by supplying water and air under pressure to the four jets upstream. As soon as the ' water on ' stage was reached, ice began to form on all the blades in the cascade and heat was immediately applied to them, in sufficient quantity to melt it, by switching on the electrical power to the test blade and by passing hot gas through the dummies. Finally, the heat input to the latter was reduced until ice was just beginning to form at their trailing edges. To determine the critical heat quantity to the test blade under these conditions it was only necessary to reduce the applied voltage until ice began to form on the surface of this blade also.

The photographs in Fig. 10, taken looking on to the concave surface from downstream, illustrate the various stages of the icing process which took place with progressive reduction of heat input. The first sign was an increase in the amount of water running back over the concave surface, eventually forming an almost continuous film and breaking up into large drops at the trailing edge. When the heat was further reduced, one of these would freeze and become attached (Fig. 10b), but only for an instant; almost immediately it would be dislodged and whisked away downstream. Then, after a second or two, another similar transitory group of crystals would appear in almost the same spot, only in turn to be blown away. When the heat input was kept constant at this value the cycle would repeat itself with almost constant frequency. However, as this did not represent true icing, the power was again reduced, and the cycle of crystallization and blow-off was seen to change, the particles adhering longer and reappearing after shorter intervals (Fig. 10c). With still further reduction of heat a point was reached when the ice attached to the trailing edge was not dislodged by the air stream but, instead, began to grow forward continuously. In Fig. 10d, which illustrates the beginning of this stage, the ice can be seen attached only at the trailing edge, while in Fig. 10e after another slight reduction of heat it is clearly growing over a large part of the concave surface. This change of behaviour characterised by the appearance of a continuously spreading ice film at the trailing edge was used in the tests as an indication of when the critical heat quantity had been reached.

Throughout the range of heat input corresponding to Figs. 10a to 10d there was no ice on the leading edge of the blade, but when the stage in Fig. 10e was reached it had already formed independently on both the trailing and leading edges and was growing forward from the one and backward from the other. Without further heat reduction this growth continued until the whole of the concave surface of the blade was covered and eventually the blade took on the appearance illustrated in Fig. 10f. In the earlier stages very little ice formed on the convex surface but, when this final stage was reached, a thin film of ice began to grow forward from the trailing edge. The deposit was, however, always much less than that on the concave surface, which was subject to direct impact of the water droplets.

The ice formation under other external conditions is illustrated in Fig. 9; the same stages of growth are apparent. Fig. 9b represents a stage just before the critical point is reached; Fig. 9c after further heat reduction with ice at both leading and trailing edges, while Figs. 9d and 9e show the subsequent build up. Both Figs. 9 and 10 show quite clearly that the ice deposit on an insufficiently heated blade is concentrated near the trailing edge in contrast to that on an unheated blade which is thickest at the trailing edge. In the former case, once ice has begun to form at the trailing edge, it acts as a water trap; it increases the local catch of airborne water particles and at the same time forms a barrier to the water flowing downstream from the centre of the blade where the surface temperature is slightly higher. Also the surface irregularity, formed by the ice at the trailing edge, causes an increase in the local heat transfer, which, in conjunction with the local restriction on internal heat flow due to the thin section, produces a drop in the local temperature and a further tendency towards freezing.

5.3. *Effects of Air Velocity and Icing Conditions.*—The external conditions to which the critical heat quantity is theoretically related are:

(*a*) air velocity, V_1, upstream of the cascade

(*b*) Icing conditions:

(i) effective air temperature, t_1'

(ii) water concentration, n

(iii) droplet diameter, d.

The effect upon the critical heat quantity of variation of each of these parameters was investigated experimentally, using the procedure outlined above; for stator blades at values of incidence of + 10 deg, 0 deg and — 10 deg, and for inlet guide vanes at 0 deg.

It was found that the heat input, H_e, with trailing-edge icing, varied linearly with the effective air temperature, t_1', but that the curves, as shown in Fig. 11, when extrapolated did not pass through the origin, suggesting that with temperatures a few degrees below zero no heat would be required to maintain the blades free from growing ice. This is not surprising when it is remembered that with the critical heat input as measured, ice was continuously being formed at the trailing edge and blown off. As the drops of water froze the latent heat of fusion was liberated and although part of it was dissipated by convection, some was probably transferred to the blade, which locally must have had a temperature slightly lower than zero. According to this supposition the discrepancy would increase with the amount of water caught, and in fact this is so, as is shown by the quantitative analysis in Appendix II and in Table 6.

Although the critical heat quantity was not exactly proportional to $(0 - t_1')$ over the wide range of temperature, it is convenient and not very inaccurate to assume proportionality in the analysis of test results obtained over a small range of temperature. In the remaining figures, therefore, the critical heat quantity, H_e, is combined with the external blade surface area, S_a, and the effective air temperature, t_1', to form the parameter $H_e/S_a\ (0 - t_1')$, which is analogous to a heat-transfer coefficient and is related theoetically to the true heat-transfer coefficient in dry air. This factor is plotted in Figs. 12, 13a and 13b against air velocity, V_1, water concentration, n, and droplet diameter, d. It varies as $V_1^{0.8}$, is linear with respect to n, and is apparently independent of d over the range of tests. Incidence, i, has only a small effect and that is most clear in the figures dealing with variations of n. The reasons for these relationships and a comparison between these results and the theory are given in the following section.

Besides the trailing-edge icing condition two others were investigated: icing at both trailing and leading edges in Fig. 12b, and the blade completely free of ice in the case of the I.G.V. in Fig. 13. From these curves the corresponding values of heat input under the same external conditions can be obtained. With ice at both edges the heat input is 20 per cent lower than the trailing edge critical value, while with a completely ice-free blade it is 26 per cent higher.

5.4. *A Comparison with Theory.*—The heat required to prevent the formation of ice on an aerofoil can be calculated theoretically by the method given in Ref. 3.

For the purpose of analysis the heat dissipated by an element of heated surface, ΔS_a, subject to icing conditions may be divided into these three parts:

ΔH_1 = heat dissipated by convection

ΔH_2 = heat dissipated by evaporation of water from the surface

ΔH_3 = heat dissipated in raising the temperature of the water striking the surface up to the surface temperature.

These three components each depend upon their local conditions. ΔH_1 and ΔH_2 can be combined to give:

$$\Delta H_1 + \Delta H_2 = h(t_s - t_3') + 0{\cdot}622 \frac{L_s}{c_p} \frac{(e_s - e_3)}{p_3} S_a, \quad .. \quad .. \quad .. \quad (7)$$

where

h = local heat-transfer coefficient

t_s = local surface temperature

t_3' = local effective air temperature just outside the boundary layer

$= t_{\text{tot}} - 0{\cdot}16 V_s^2/2gJc_p$

L_s = latent heat of vaporisation at t_s

c_p = specific heat of air at constant pressure

e_3 = local vapour pressure just outside the boundary layer

e_s = saturation vapour pressure at t_s

p_3 = local static pressure.

Equation (7) cannot be applied directly to a compressor blade in the form presented unless the local values of t_3', e_3 and p_3 over the whole surface are known. To determine the heat dissipation due to convection and evaporation in that case, it is only necessary to put $t_3 = 0$ in the equation and to integrate over the whole surface. However, a detailed calculation of the chordwise variation of t_3, e_3 and p_3 over a blade similar to the ones used in the tests, under similar conditions, reveals that the term

$$(t_s - t_3') + 0{\cdot}622 \frac{L_s}{c_p} \frac{(e_s - e_3)}{p_3}$$

is roughly a constant over the whole blade for a given set of external conditions, and that the greater variation is in the local heat-transfer characteristic, h. The integration can, therefore, be simplified if a representative value of this parameter is used in conjunction with the overall mean heat-transfer coefficient for the blade. For convenience in the calculations the representative temperature is taken as the effective temperature, t_1', just upstream of the blade. This is a fairly close approximation to a mean value of t_3', for the velocity change through the cascade was not very great in either the stators or the inlet guide vanes, and the mean velocity was probably fairly close to V_1. As the same argument applies for the static pressure and the vapour pressure, the suffix 3 in equation (7) can be replaced throughout by 1 to give an integration:

$$H_1 + H_2 = h_m(t_s - t_1') + 0{\cdot}622 \frac{L_s}{c_p} \frac{(e_s - e_1)}{p_1} S_a, \quad .. \quad .. \quad .. \quad (8)$$

where

h_m = overall mean heat-transfer coefficient

S_a = total blade-surface area in the airstream.

The vapour pressure, e_1, is calculated on the assumption that there is no change of state from liquid to vapour as the air is accelerated up to the blades, so that:

$$e_1 = e_0 \frac{p_1}{p_0} \qquad (9)$$

where p_0 and e_0 are the static air pressure and the saturation vapour pressure corresponding to the temperature t_0.

The overall heat-transfer coefficients used in the calculations were found experimentally by measuring the heat input necessary to maintain the surface temperature of the electrically heated blades at 0 deg C in a dry air stream at a temperature of — 20 deg C. A range of air velocities was covered and the results were plotted as Nusselt number, Nu, against Reynolds number Re_1, on a logarithmic basis. These parameters are defined as:

$$Nu = \frac{h_m c}{\lambda} \qquad (10)$$

$$Re_1 = \frac{V_1 c \rho_m}{\mu} \qquad (11)$$

where

c = blade chord

λ = conductivity of air at t_1

μ = viscosity of air at t_1

ρ_m = density based on the mean of pressures upstream and downstream and on t_1.

Two sets of points are shown in Fig. 14a, one for the stator blade and the other for the inlet guide vane, both at zero incidence; they all lie close to the straight line representing the relationship:

$$Nu = 1{\cdot}90 \times 10^{-2}(Re_1)^{0{\cdot}8}. \qquad (12)$$

The third heat component, H_3, is calculated for the whole blade. It is given by the equation:

$$H_3 = G_w(t_3 - t_w). \qquad (13)$$

The amount of water caught, G_w, depends upon the projected area of the blade normal to the airflow upstream of the cascade, S_p, the velocity, V_1, and the water concentration, n. The projected areas of the stator blades are tabulated in Fig. 2 which shows the direction of airflow at each of the three incidences. The projected area of the inlet guide vane was the same as that of the zero-incidence stator.

The amount of water impinging on the blade is not, however, exactly equal to that passing through the corresponding projected area, but rather some fraction, η_c, of the quantity. This factor is called the efficiency of catch and according to the theory of M. Glauert[4], is dependent upon droplet size and Reynolds number.

Assuming, then, that the water droplets are still at a temperature, t_1', on reaching the blades, we have:

$$H_3 = \eta_c V_1 n S_p (t_s - t_1'). \quad \ldots \quad \ldots \quad \ldots \quad \ldots \quad \ldots \quad (14)$$

However, the theoretical values of η_c exceed 0·95 for all conditions of test with droplet sizes above 15 microns diameter. Therefore, in calculating the theoretical heat requirement, an efficiency of catch of 100 per cent is assumed and the following formula, which is obtained by adding equations (8) and (14) and replacing t_s by 0, is used:

$$H_c = H_1 + H_2 + H_3 = h_m \left[(0 - t_1') + 0{\cdot}622 \frac{L_s}{c_m} \frac{(4{\cdot}58 - e_1}{p_1} \right] S_a + V_1 n S_p (0 - t_1'). \quad (15)$$

The theoretical curve of H_c versus V_1 for stator and inlet guide vanes is shown in Fig. 14b together with the test figures which all lie fairly close. The experimental values, H_e, are roughly 10 per cent higher than the theoretical values, H_c, but since the electrically heated blades were less than 100 per cent efficient, the real difference between the theoretical estimate and the requirement of a blade with uniform surface temperature may be less than this figure. The conclusion is that this method gives a good practical estimate of the critical heat quantity.

6. *Anti-Icing by Gas Heating.*—Although electrical heating has proved to be highly efficient the weight penalty may be high, and where hot gas is available this may be a more acceptable means. The feasibility of gas heating as a method of anti-icing depends upon the limitations of mass flow and pressure available from the engine. The gas may, of course, be air, as when a compressor is tapped, but to avoid confusion the term ' gas ' is used throughout this paper to designate the heating medium.

6.1. *The Gas-Heated Blades.*—The arrangement for gas heating as used in the tests was quite simple. Compressed air from the house supply, after passing through a throttling valve and metering section, flowed along an insulated tube with a coaxial heating element of 1 kilowatt capacity, capable of heating the small quantity of air required to any temperature up to 300 deg C. From the heater the air, or rather the gas as it will now be called, passed directly into the blade via a short length of copper pipe as shown in Fig. 15. Just before the blade the gas inlet temperature, t_{g1}, was recorded by a copper-constantan thermocouple, the gas outlet temperature t_{g2}, being recorded by a mercury-in-glass thermometer.

The procedure for obtaining a measure of the critical heat quantity for the gas-heated blades was the same as that previously described for the electrically heated blades in Section 5.2, except that in this case the control of heat input to the test blade was by adjustment of the gas flow, G_g, or of the electrical input to the gas heater. After setting and recording the external conditions, the gas flows to the test blade and the dummies were reduced until icing occurred simultaneously at the trailing edges of all the blades. A record was then made of G_g, t_{g1}, t_{g2} and P_{g1}, the gas pressure before the blade.

To obtain information regarding the effect of blade passage configuration and blade material, ten different blades, having a variety of internal shapes, were tested. For ease of reference they were given letters of the alphabet indicating this shape. Six of them are illustrated in Fig. 16, and the internal dimensions of nine are given in Fig. 17. The tenth blade was hollow with no baffle but was packed with steel wool; although the thermal efficiency was fairly good the pressure loss was so high that the blade was obviously impracticable.

Some of these blades were mounted in the stator cascade while others were used as inlet guide vanes, but when comparing thermal efficiencies this is irrelevant as values are obtained by comparing the heat input to electrical and gas-heated blades of the same type.

6.2. *Thermal Efficiencies.*—As opposed to electrical heating, where the heat output per unit length of the element is constant, the heating value per unit length of internal gas passage is dependent upon the local internal heat-transfer coefficient and the gas temperature. Hence, it is difficult to design a blade in which all the heat goes where it is most required and this lack of control over the heat distribution means local overheating and poor thermal efficiency. Also, the gas, on leaving the blade, carries away a certain amount of the heat supplied, still further reducing the efficiency.

There are several ways in which thermal efficiency may be expressed depending upon how the heat input is defined. Each expression is obtained by dividing the heat required by a blade of 100 per cent efficiency, which in these tests is assumed to be the electrically heated blade, by the input to the gas heated blade under the same external conditions, two of the most useful expressions are:

$$\eta' = \frac{H_e}{G_g c_{p\,g}(t_{g\,1} - t_b)} = \text{utilization efficiency} \quad .. \quad .. \quad .. \quad (16)$$

$$\eta'' = \frac{H_e}{G_g c_{p\,g}(t_{g\,1} - t_{g\,2})} = \text{distribution efficiency} .. \quad .. \quad .. \quad (17)$$

where G_g = gas mass flow through the blade

$c_{g\,p}$ = specific heat of the gas

t_b = blade surface temperature.

The utilization efficiency is more important when estimates of feasibility of gas heating are being made, since the heat input is related to a fixed datum temperature, t_b, which is usually taken as 0 deg C. It will be noted that for $t_b = 0$ deg C:

$$\eta' = \eta'' \frac{(t_{g\,1} - t_{g\,2})}{t_{g\,1}} . \quad .. \quad .. \quad .. \quad .. \quad .. \quad .. \quad (18)$$

Of these two terms, the first, η'', is a measure of the effectiveness of the heat distribution over the blade surface; when all the heat goes where it is required the surface tempearture is uniform and η'' is 100 per cent. The second, the temperature ratio, is a measure of the heat given up by the gas during its passage through the blade divided by that which it would give up if cooled to the surface temperature. The former is chiefly a function of blade metal conductivity and passage configuration; the latter, of gas Reynolds number and ratio of total passage length to mean diameter.

The thermal efficiencies of nine gas heated blades are plotted in Fig. 18 against Reynolds number of the internal gas flow, Re_g, which is defined by:

$$Re_g = \frac{4G_g}{\mu_g Z_g} \quad .. \quad .. \quad .. \quad .. \quad .. \quad .. \quad .. \quad (19)$$

where μ_g = viscosity of the gas at blade temperature

Z_g = mean periphery of the internal passage.

Three of the steel blades tested were of the Z-flow type in which the gas transversed the blade three times before leaving it. The first of these tested was Z_1 (*see* Fig. 16), which was of stainless steel and fitted with two wide baffles. These were arranged so that theoretically the internal chordwise distribution of heat transfer corresponded roughly to the external distribution of heat dissipation necessary to maintain the whole surface temperature at 0 deg C. At $Re_g = 10^4$ the distribution efficiency was, however, only 38 per cent. During the test, ice formed at the trailing edge while the centre was almost dry, a sure indication that too much heat was being liberated in the middle passage. In the next blade the cross-sectional area of this passage was increased

in relation to the other two, the thick baffles being replaced by thin sheet material. On testing the new blade, Z_2, a large improvement was immediately evident; the distribution efficiency had increased to 62 per cent. This was, in fact, the best performance of an all-steel blade, and further adjustment of the baffles as in Z_3 only reduced the efficiency. The distribution efficiency of each Z-flow blade was almost constant but the utilization efficiency decreased rapidly with increase in Re_g. For the Z_2 blade at the value $Re_g = 10^4$ the utilization efficiency was 42 per cent.

Three other types of steel blades were used, U-flow, E-flow and I-flow, the last named being a simple hollow blade without baffles. The utilization efficiencies of all of these were very low and their value lies chiefly in the low gas-pressure loss associated with their use. The U-flow blade which is illustrated in Fig. 16 had one baffle down the middle and the gas was introduced at either the leading or the trailing edge; the suffixes $_{\text{L.E.}}$ and $_{\text{T.E.}}$ indicate which type of flow is intended. The performance of $U_{\text{L.E.}}$ was very disappointing; the ice stayed on the trailing edge in large lumps when the leading edge was obviously quite warm. Reversing the gas inlet and outlet improved the performance, but the trailing edge still iced while the centre of the blade remained clear. It was obvious that the control of heat distribution afforded by one baffle was insufficient and this type of blade was not investigated further. Instead, attention was turned to the single-pass blades E and I, as shown in Fig. 16, the former being simply a converted Z_1 blade. Of these two the E-flow blade was superior to the I, its utilization efficiency at $Re_g = 10^4$ being 14·5 per cent as against 9 per cent for the latter. With these simple single-pass blades there was no means of influencing the chordwise distribution of heat transfer and, in maintaining the trailing edges ice-free, the other parts were considerably overheated. The distribution efficiencies were, therefore, very low, 29 per cent for the E-flow and 18 per cent for the I-flow. There is little doubt that by suitable internal finning these figures could have been improved, but another method was being investigated and this line was not taken up.

All the blades so far described were of steel and their temperature distributions during icing were comparatively poor. To determine the effect of surface conductivity on temperature distribution a copper blade was made geometrically similar to Z_1 described above. When this blade was put to the test a startling improvement over Z_1 in steel was observed. It was found that the distribution efficiency of the copper blade, Z_1Cu, was 100 per cent and over. In other words, its temperature distribution was as good as, and under certain conditions, better than, that obtained with the electrically heated blades. The highest value of utilization efficiency obtained throughout the tests was with this blade; at $Re_g = 10^4$ the value of η' was 74 per cent. This improvement with the three-pass blade suggested the application of copper to the simple straight-through blades, but as copper itself is a soft metal it was decided to copper-plate a steel blade to obtain a strong blade with a high surface conductivity. A converted U-flow blade with the end plate removed was, therefore, plated and then cleaned to leave a layer of roughly 0·030 in. of copper over the surface. The blade was tested, 0·015 in. of copper removed, and tested again. The distribution efficiencies of these copper plated blades were 67 per cent and 55 per cent respectively as compared with 18 per cent for a hollow steel blade. As a result of the good temperature distribution the corresponding values of utilization efficiency were 43 per cent and 34 per cent at $Re_g = 10^4$, which puts these blades in the same class as the Z-flow blades without their having the same high associated pressure loss.

6.3. *Internal Heat Transfer.*—It has been shown that the utilization efficiency, η', is the multiple of two terms, the distribution efficiency, η'', and the temperature ratio $(t_{g\,1} - t_{g\,2})/t_{g\,1}$. The latter is a function of the heat transfer between the gas and the blade which is dependent upon the Reynolds number, Re_g, and the internal passage dimensions. A useful method of expressing the internal heat transfer when effect of scale is being considered is demonstrated in Appendix III where it is shown that, when a gas flows through a tube of constant cross-section at a constant surface temperature, t_s, the relationship between the inlet and outlet gas temperatures is given by the expression:

$$\frac{t_{g\,1} - t_s}{t_{g\,2} - t_s} = \exp \frac{4Nu}{Pr\,Re} \frac{L}{D}. \qquad \ldots \ldots \ldots \ldots \quad (20)$$

Assuming the theoretical relationship between Nu and Re for fully developed flow:

$$Nu = 0{\cdot}023 Pr^{0{\cdot}4}\, Re^{0{\cdot}8}, \quad .. \quad .. \quad .. \quad .. \quad (21)$$

this expression becomes:

$$\frac{t_{g\,1} - t_s}{t_{g\,2} - t_s} = \exp 0{\cdot}113\, Re^{-0{\cdot}2}\, \frac{L}{D} \ldots \quad .. \quad .. \quad .. \quad (22)$$

For a blade being tested under icing conditions $t_s \simeq 0$ deg C. Hence the equivalent relationship is:

$$\frac{t_{g\,1}}{t_{g\,2}} = \exp 0{\cdot}113\, Re_g^{-m}\, \frac{L_g}{D_g}. \quad .. \quad .. \quad .. \quad (23)$$

The actual relationship between $t_{g\,1}/t_{g\,2}$, L_g/D_g and Re_g for the gas-heated blades is shown in Fig. 19. Again there is an appreciable discrepancy between these and the theoretical one. However, in all cases the curves indicate a relationship of the form:

$$\frac{t_{g\,1}}{t_{g\,2}} = \exp K\, Re_g^{-m}\, \frac{L_g}{D_g}, \quad .. \quad .. \quad .. \quad .. \quad (24)$$

where the values of K and m are those given in Table 2.

It is evident that K and m depend chiefly upon the shape and distribution of the internal passages and it is very likely that two blades with geometrically similar passages will have approximately the same values. For a blade scaled up equally in all directions, therefore, the same relationship between $t_{g\,1}/t_{g\,2}$ and Re_g will hold good.

6.4. *The Conduction Factor.*—The distribution efficiency, as the name implies, is a measure of the effectiveness of heat distribution over the blade surface. As the tests show, high efficiency can be obtained both by designing the passages to match internal and external heat transfer, and by facilitating the flow of heat in the skin by using a high-conductivity material. The former means depends upon the internal shape, the latter upon the metal conductivity and thickness. In analysing the results the problem is to separate the two effects.

One method is suggested by the theory given in Appendix IV. If a strip of material is heated at one end and subjected to uniform icing conditions all along one side (Fig. 21), it is shown that the distribution efficiency is theoretically related to a chordwise conduction factor:

$$\gamma = \left(\frac{h_a' l^2}{\Sigma \lambda_m \delta}\right)^{1/2} \quad .. \quad .. \quad .. \quad .. \quad .. \quad .. \quad .. \quad (25)$$

where

h_a' = equivalent heat-transfer coefficient

$$= \frac{H_e}{S_a(0 - t_1')}$$

δ = metal thickness

$\Sigma \lambda_m$ = effective metal conductivity

l = length of the strip.

The theoretical relationship between η'' and γ is:

$$\eta'' = \frac{\gamma}{\sinh \gamma} \simeq \frac{1}{1 + \gamma^2/6}. \quad .. \quad .. \quad .. \quad .. \quad .. \quad (26)$$

Now the heat conduction in the metal skin of the blade is analogous to that described in this simple case, with the difference that the heat is not applied at one section but on several regions. The equivalent value of l, therefore, must be a function of the internal geometry, corresponding to a mean distance between the region where the heat is applied and the region where it is required. It will obviously be least where the internal and external heat-transfer coefficiencts are ideally matched, for it will then be zero.

The experimental results for Z_1 and Z_1Cu (Fig. 21), which have the same shape and, therefore, the same value of l, fit a curve of the form represented by equation (26) when $l/c = 0{\cdot}40$ (except that η'' is replaced by $\eta''/1{\cdot}084$ due to the fact that the electrically heated blade is not 100 per cent efficient). This shows that the relationship holds for the blades if the correct value of l is chosen. Further, as the equation is based on a simple generalisation it should also apply to the other blades. On this assumption the equivalent values of l for other types are calculated using the experimental values of η''.

Since the gas passages run along the length of the blades and the greatest temperature differences occur in the chordwise plane, the representative distance, l, must be proportional to the blade chord. Therefore the values of l/c are tabulated for the various types of blade and effect of scale change may be allowed for by multiplying by the new chord length.

6.5. *Pressure Loss.*—One of the limitations to gas heating is the relatively high pressure required to force the gas through the hollow blades, particularly those with more than one passage in series. When the tests described in this paper were initiated the full importance of the pressure loss was not realised and no attempt was made to design test blades with smooth entries. As the sketches in Fig. 16 show, the hot gas was introduced through relatively small holes causing greater inlet losses than necessary. In an engine the blade inlets would no doubt be flared, and the loss figures for the test blades may, therefore, be conservative in this respect.

The pressure drop of the gas in flowing through a blade is made up of two parts, one due to frictional loss in the straight passages and the other to losses at the entry, at the bends, and at the exit. It would have been difficult to measure these separately and it was considered sufficient for the purpose of these tests to determine the total pressure drop Δp_g. For the types of blade used the losses due to rapid changes of section and sharp bends are large compared with the frictional losses, and small differences in inlet shapes and lengths of baffle make enormous differences to the total pressure drop. A comparison in Fig. 20a of the pressure drops through Z_1Cu and Z_1, which were geometrically identical and which had the same heat-transfer characteristic, demonstrates this very clearly. It should be remembered, therefore, that the empirical expressions for pressure drop, deduced in this section apply only to these particular forms and that intelligent modification of the internal shape might reduce the losses in some, if not all of the blades shown.

The theoretical expression for the pressure drop due to friction in a length dl of passage is:

$$d'p_g = fq\frac{Z}{A}\,dl, \qquad \ldots\ldots\ldots\ldots\ldots\ldots\ldots \quad (27)$$

where f is the resistance coefficient and q the velocity head. As f and q change as the gas flows through the blade, mean values must be taken, thus:

$$\Delta'p_g = f_m q_m \frac{Z_g}{A_g} L_g\,. \qquad \ldots\ldots\ldots\ldots\ldots\ldots\ldots \quad (28)$$

The pressure loss at the corners and at inlet may also be expressed in terms of the mean velocity head:

$$\Delta''p_g + \Delta'''p_g = \alpha q_m + \beta q_m\left(\frac{A_g}{A_i}\right)^2, \qquad \ldots\ldots\ldots\ldots\ldots\ldots\ldots \quad (29)$$

where A_i is the cross-sectional area of the inlet to the blade. The second term is the inlet loss, the area ratio representing the ratio of inlet to mean velocity. The three terms can be combined to give:

$$\frac{p_{g\,m}\Delta p_g}{G_g^2}\frac{2_g}{R_g T_{g\,m}} = \frac{1}{A_g^2}\left\{f_m\frac{4L_g}{D_g} + \alpha + \beta\left(\frac{A_g}{A_i}\right)^2\right\} \quad \ldots \quad (30)$$

In Fig. 20 this function of pressure loss is plotted against Reynolds number. There were, obviously, no bend losses in the I-flow blade and it was possible to estimate the inlet loss by subtracting from the measured total, the theoretical friction. Applying this value to some of the other blades, which had similar types of gas inlet, a rough estimate was made of relative values of their various pressure-drop components when $Re_g = 10^4$.

6.6. *Summary of the Empirical Equations.*—In the last three subsections the heat transfer and pressure drop through the blades have been analysed. The results can be summarised by the following equations.

The heat transfer results give:

$$\frac{t_{g\,1} - t_{g\,2}}{t_{g\,1}} = 1 - \exp\left[-K\,Re_g^{-m}\frac{L_g}{D_g}\right] \quad \ldots \quad (31)$$

and

$$\eta'' = \frac{1{\cdot}084}{1 + (h_a' l^2)/(6\Sigma\lambda_m\delta)} \quad \ldots \quad (32)$$

Now from equation (17):

$$G_g = \frac{H_e}{\eta'' c_{p\,g}(t_{g\,1} - t_{g\,2})}, \quad \ldots \quad (33)$$

so that substituting from equations (19) and (33) and rearranging we get:

$$Re_g\left[1 - \exp\left(-K\,Re_g^{-m}\frac{L_g}{D_g}\right)\right] = \frac{4H_c}{c_{p\,g}\mu_g Z_g t_{g\,1}}\frac{1}{\eta''} \quad \ldots \quad (34)$$

The term $1{\cdot}084$ appears in the equation for η'' because H_e is greater than the heat required by a 100 per cent efficient blade. If the ideal value, H_c, is used then η'' should be replaced by $\eta''/1{\cdot}084$ so that:

$$Re_g\left[1 - \exp\left(-K\,Re_g^{-m}\frac{L_g}{D_g}\right)\right] = \frac{4H}{c_{p\,g}\mu_g Z_g t_{g\,1}}\left\{1 + \frac{h_a'\,(l/c)^2\,c^2}{6\,\Sigma\lambda_m\delta}\right\} \quad \ldots \quad (35)$$

In a similar way Δp_g may be expressed in terms of Re_g by substituting from equation (19) in equation (30).

Then

$$p_{g\,1}^2 - p_{g\,2}^2 = \frac{Re_g^2 R_g T_{g\,m}\mu_g^2}{g D_g^2}\left(f_m\frac{4L_g}{D_g} + B\right), \quad \ldots \quad (36)$$

where

$$T_{g\,m} = t_{g\,1}\left[\frac{1 + \exp\{-K\,Re_g^{-m}\,(L_g/D_g)\}}{2}\right] + 273 \quad \ldots \quad (37)$$

and

$$f_m = 0{\cdot}079\,Re_g^{-0{\cdot}25}\ \text{(Blasius)}. \quad \ldots \quad (38)$$

In these expressions K, m, l/c and B are non-dimensional empirical coefficients which are tabulated for the test blades in Tables 2, 3 and 4.

In Appendix V a specimen calculation is presented where the test results have been extrapolated to cover the case of a larger size blade having the same form and geometrical shape as one of the test blades. The same values of the various parameters are assumed to apply to the scaled up blade as do to the similar test blade.

For the purpose of this specimen calculation, the number of variables has been reduced by choosing one particular engine flying under known conditions, assuming that a compressor bleed is used for anti-icing a row of inlet guide vanes. In order to draw any conclusions as to the feasibility of a system of anti-icing it would be necessary to do many such calculations for various conditions of flight.

7. *Conclusions.*—(*a*) Electrical heating is a thermally efficient means of protecting compressor blades from ice accretion. By suitable arrangement of heating elements an almost uniform surface temperature can be obtained under icing conditions. The electrically heated blades used in the tests had a total surface temperature variation of about 2·5 deg C, in an air stream at — 2·5 deg C, the coldest part being the trailing edge, and required approximately 10 per cent more heat than the ideal blade with uniform surface temperature. This was, however, a copper blade which would be unsuitable for aircraft application. A drop in efficiency is to be expected if steel or aluminium electrically heated blades are used.

(*b*) Under conditions obtained, the critical heat quantity as defined in section 5.2 was:

(i) proportional to the upstream velocity to the power 0·8

(ii) approximately proportional to the effective air temperature below zero

(iii) approximately linear in relation to water concentration

(iv) independent of droplet size.

(*c*) The theoretical method of J. K. Hardy is a reasonably accurate means of calculating the critical heat quantity.

(*d*) Gas-heated blades are thermally inefficient. There are two causes; one is the non-uniformity of surface temperature due to lack of control over heat distribution, and the other the heat lost with the escaping gas. The former is improved by better matching of the internal and external heat-transfer coefficients and by increasing the conductivity of the blade material; the latter by increasing the length to diameter ratio of the internal gas passage and by decreasing the internal Reynolds number. By careful design of blade and suitable choice of materials great improvements in the performance of the gas-heated blade may be obtained.

Acknowledgment.—The authors are indebted to Mr. D. G. A. Rendel and Mr. F. J. Bigg of the R.A.E., whose advice and assistance have been of great value.

NOTATION

Blade Configuration

c		Blade chord	ft
s		Blade pitch	ft
L		Length in air stream	ft
Z		External periphery	ft
S_a	=	ZL Surface area	ft^2

Y		Projected width	ft
S_p	=	YL Projected area	ft^2
i		Incidence	deg

External Conditions

V		Air velocity	ft/sec
t		Static air temperature	deg C
t'	=	$t_{tot} - 0{\cdot}16V^2/2gJc_p$ Effective air temperature	deg C
t_{tot}		Total air temperature	deg C
T		Air temperature	deg C
p		Static air pressure	lb/ft^2
p_{tot}		Total air pressure	lb/ft^2
n		Water concentration	gm/m^3
d		Mean droplet diameter	microns
t_w		Water temperature	deg C
ρ		Air density	lb/ft^3

Suffices Referring to the Icing Tunnel

0	Conditions before the accelerator
1	Conditions before the cascade
2	Conditions after the cascade

External Heat Transfer

t_s		Local surface temperature	deg C
t_b		Mean blade surface temperature	deg C
e		Vapour pressure	mm Hg
L_f		Latent heat of fusion of ice	CHU/lb
L_s		Latent heat of evaporation of water	CHU/lb
G_w		Rate of water catch	lb/sec
x		Percentage of water freezing	per cent
h		Local convective external heat-transfer coefficient	CHU/ft^2 sec deg C
h_m		Mean convective external heat-transfer coefficient	CHU/ft^2 sec deg C
X		Ratio of evaporative to convective heat transfer	
η_c		Efficiency of catch	

Suffix

3		Local conditions just outside the boundary layer
Re_1	=	$(V_1 c \rho_m)/\mu$ Reynolds number (external)
Nu	=	$(h_m c)/\lambda$ Nusselt number (external)

c_p		Specific heat of air	CHU/lb deg C
μ		Viscosity of air (at t_1)	lb/ft sec
λ		Conductivity of air (at t_1)	CHU/ft sec deg C
ρ_m		Mean density based on $(p_1 + p_2)/2$ and t_1	lb/ft^3

Surface Heating

H_c		Critical heat quantity	CHU/sec
H_e		Heat to electrically heated blade	CHU/sec
h_a'	=	$H_e/S_a(0 - t_1'')$Effective external heat-transfer coefficient	CHU/ft^2 sec deg C
t_g		Gas temperature	deg C
T_g		Gas temperature	deg K
Δt_g		Temperature drop through blade	deg C
p_g		Gas pressure	lb/ft^2
Δp_g		Pressure drop through blade	lb/ft^2
G_g		Gas mass flow	lb/sec
c_{pg}		Specific heat of the gas	CHU/lb
η'	=	$H_e/\{G_g c_{pg}(t_{g1} - t_b)\}$ Utilization efficiency	
η''	=	$H_e/\{G_g c_{pg}(t_{g1} - t_{g2})\}$ Distribution efficiency	

Suffices

1	Conditions at inlet to the blade
2	Conditions at outlet from the blade

Dimensions of the Gas-Heated Blades

L_g		Total length of gas passage	ft
A_g		Mean cross-sectional area of passage	ft^2
A_i		Cross sectional area of inlet	ft^2
Z_g		Mean periphery of passage	ft
D_g	=	$4A_g/Z_g$ Mean hydraulic diameter	ft
S_g	=	$Z_g L_g$ Total internal surface area	ft^2

Internal Heat Transfer

h_g		Mean internal heat-transfer coefficient	CHU/ft^2 sec deg C
q_m		Mean internal velocity head	lb/ft^2
Re_g	=	$4G_g/(\mu_g Z_g)$ Reynolds number (internal)	
Nu_g	=	$(h_g D_g)/\lambda_g$ Nusselt number (internal)	
Pr_g	=	$(\mu_g c_{pg})/\lambda_g$ Prandtl number (gas)	
μ_g		Viscosity of gas (at t_b)	lb/ft sec

λ_g		Conductivity of gas (at t_b)	CHU/ft sec deg C
f		Friction coefficient	
γ	=	$\sqrt{\{(h_a{}^1l^2)/(\Sigma\lambda_m\delta)\}}$ Conduction factor	
λ_m		Metal conductivity	CHU/ft sec deg C
δ		Metal thickness	ft
l		Representative length	ft

l/c, K, m and B are non-dimensional coefficients determined experimentally for each type of blade, where:

$$\frac{t_{g1}}{t_{g2}} = \exp K\, Re^{-m} \frac{L_g}{D_g}$$

$$\text{and } \Delta p_g = f_m \frac{4L_g}{D_g} + B$$

REFERENCES

No.	*Author*	*Title, etc.*
1	J. K. Hardy	Evaporation of drops of liquid. R. & M. 2805. March, 1947.
2	A. R. Jones and W. Lewis ..	Recommended values of meteorological factors to be considered in the design of ice prevention equipment. N.A.C.A. Tech. Note 1855. March, 1949.
3	J. K. Hardy	Protection of aircraft against ice. R.A.E. Report. S.M.E. 3380. A.R.C. 10,034. July, 1946.
4	M. Glauert	A method of constructing the paths of raindrops, etc. R. & M. 2025. November, 1940.
5	W. H. McAdams	*Heat Transmission.* McGraw-Hill Book Company.

APPENDIX I

Calculation of Droplet Temperature

As the water drops from the jets are carried downstream their temperature, t_w, is reduced as heat is dissipated from them by convection and evaporation. The value when they reach the working section is unknown, but can be calculated approximately.

Theoretically[1], the rate of cooling of a drop of water in still air is a function of its diameter, d, and the temperature of the air, t. The time taken to cool from $t_{w\,1}$ to $t_{w\,2}$ is given by:

$$\tau = \frac{d^2 \rho_w c_{p\,w}}{12\lambda(1 + X)} \log_e \frac{(t_{w\,1} - t)}{(t_{w\,2} - t)}, \quad .. \quad .. \quad .. \quad .. \quad (39)$$

where

ρ_w = density of water

$c_{p\,w}$ = specific heat of water

λ = air conductivity at t_w

X = ratio of evaporative to convective heat transfer.

In the tunnel the drops have a velocity relative to the air stream initially but negligible after a short interval of time. The actual cooling rate would, therefore, be higher than that in still air.

Since λ and X both vary with t_w, the total temperature drop being considered is divided into small parts, and the mean values of these parameters calculated for each step. The total cooling time is then the sum of the cooling times over each step. As an example, the time taken by a drop of 20 microns diameter in cooling from + 50 deg C, which represents the maximum temperature of the preheated water, to — 19·9 deg C, in air at — 20 deg C has been calculated. The temperature drop was divided as shown in Table 5 and the separate time elements calculated.

The maximum velocity in the parallel section of the tunnel was 50 ft/sec so that the minimum time of transit through the 5 ft length was 0·10 sec. This is a longer period than covered by the table and it is clear that the droplet temperature at the end of the parallel section must have been very close to the static temperature, t_0, which, in turn, was within 0·1 deg C of the total temperature t_{tot}. It is, therefore, safe to assume that before the accelerating section $t_w = t_{tot}$.

After the parallel section the tunnel walls converged sharply and the air static temperature fell rapidly. The time of transit of the drops was so short, however, that theoretically their maximum temperature drop was only a fraction of the drop in air temperature. In the case considered above, for instance, the air static temperature drop was 11·5 deg C, while the calculated temperature decrease of the 20 micron drop was 1·6 deg C. The final temperature of the water on reaching the cascade was, therefore, fairly close to the effective air temperature, t_1', where

$$t_1' = t_{tot} - 0{\cdot}16 \frac{V_1^2}{2gJc_p} = -21{\cdot}85 \text{ deg C} \quad .. \quad .. \quad .. \quad (40)$$

and $t_w = -21{\cdot}6$ deg C.

APPENDIX II

The Latent Heat of Fusion

In calculations concerning completely ice-free heated blades, the latent heat of fusion can be neglected since the water arrives in the liquid state, albeit supercooled, and leaves in the same state, presumably a little above 0 deg C. However, when ice is allowed to form, either continuously growing or blown off intermittently, then the latent heat of fusion thus liberated must be added to the positive side of the heat balance equations.

Let us consider first a completely unheated blade in an air stream of effective temperature t_1', less than 0 deg C. Assuming x per cent of the impinging water to be changed to ice, the heat liberated:

$$H = xG_wL_f, \qquad \ldots\ldots\ldots\ldots\ldots\ldots\ldots \quad (1)$$

which is dissipated by convection and evaporation and by heating the water up to the blade temperature, t_b, so that:

$$xG_wL_f = [G_w + h_m(1 - X)S_a](t_b - t_1') \qquad \ldots\ldots\ldots\ldots \quad (3)$$

When

$$x = 1{\cdot}0 \text{ (rime ice)},$$

$$t_b - t_1' = \frac{G_wL_f}{G_w + h_m(1 + X)S_a}, \qquad \ldots\ldots\ldots\ldots\ldots \quad (4)$$

where

$$G_w = \eta_c V_1 S_p n\,. \qquad \ldots\ldots\ldots\ldots\ldots\ldots \quad (4.1)$$

For the blade shown in Fig. 5:

$$V_1 = 250 \text{ ft/sec}$$

$$n = 2 \text{ gm/m}^3 = 1{\cdot}249 \times 10^{-4} \text{ lb/ft}^3$$

$$S_p = 1{\cdot}31 \text{ in.}^2 = 9{\cdot}10 \times 10^{-3} \text{ ft}^2$$

and

$$\eta_c = 0{\cdot}74$$

so that

$$G_w = 2{\cdot}10 \times 10^{-4} \text{ lb/sec.}$$

It is clear from equation (4) that the blade temperature is always higher than the air temperature. However, while there is ice present it does not exceed 0 deg C, instead, when t_1' is increased above a critical temperature, t_1^*, some of the ice melts and less heat of fusion is liberated in the overall heat balance. Since X is a function of t_1' the value of t_1^* can only be found by trial and error. Assuming a value of h_mS_a for the iced blade equal to $1{\cdot}5$ times that for the uniced blade, we have for the test blade, from equation 4:

$$0 - t_1^* = \frac{2{\cdot}10 \times 10^{-4} \times 80}{2{\cdot}10 \times 10^{-4} + 1{\cdot}89 \times 10^{-2} \times 1{\cdot}51 \times 5{\cdot}64 \times 10^{-2}}$$

$$= 9{\cdot}2 \text{ deg C.}$$

When $t_1' = -9{\cdot}2$ and $t_b = 0$, the value $X = 0{\cdot}51$ applies.

When t_1' is less than $-9{\cdot}2$ deg C the blade temperature is given by:

$$t_b - t_1' = \frac{2{\cdot}10 \times 10^{-4} \times 80}{2{\cdot}10 \times 10^{-4} + 1{\cdot}89 \times 10^{-2}\,(1 + X)\,5{\cdot}64 + 10^{-3}}$$

$$\simeq 9{\cdot}2 \text{ deg C},$$

but when t_1' is greater than $-9{\cdot}2$ deg C, the blade temperature is 0 deg C and some of the ice melts. Then:

$$x = \left\{\frac{2{\cdot}10 \times 10^{-4} + 1{\cdot}89 \times 10^{-2}\,(1 + X)\,5{\cdot}64 \times 10^{-3}}{2{\cdot}10 \times 10^{-4} \times 80}\right\} \times (0 - t_1')$$

$$= \frac{0 - t_1'}{9{\cdot}2}\,.$$

These calculations are only approximate; the heat transfer coefficient h_m will also vary with the form and thickness of the ice deposit.

Next let us consider a heated blade where the latent heat of fusion affects the values of the critical heat quantity if, as in many cases, a small quantity of ice is allowed to form at the trailing edge and then to be blown off.

The curves of H_e/S_a versus t_1' in Fig. 11, when extrapolated, do not pass through the origin. It appears that if no heat is applied, the blade will remain free from growing ice at air temperatures below 0 deg C. In other words, there is a source of heat sufficient to maintain the blade temperature at about 0 deg C when the surrounding air is below zero. The source must, in fact, be the latent heat of fusion of the ice formed at the trailing edge. In Table 6 the additional heat quantity is tabulated together with the equivalent percentage of the water catch which would liberate this heat quantity on being changed to ice.

APPENDIX III

Heat Transfer in a Tube

The temperature drop through a gas-heated blade, $t_{g1} - t_{g2}$, is a function of the heat transfer from gas to metal, which is in turn dependent upon gas Reynolds number, Re, and passage dimensions. Although the passage shapes are sometimes complex, the heat transfer is analogous to that in a tube of constant circular section, and a theoretical treatment of this simple case suggests a method of analysing the test results.

Let us consider fully developed turbulent flow in a pipe of constant diameter D and total length L.

The surface temperature, t_s, is assumed to be uniform.

Over an element of length dL the heat transferred from the gas to the wall must be equal to the loss of sensible heat, so that:

$$Cc_p\, dt_g = -\, h(t_g - t_s)\pi D\, dL\,. \qquad (4.2)$$

Let

$$t_g - t_s = \theta\,, \text{ then:}$$

$$Gc_p\, d\theta = -\, h\theta\pi D\, dL\,,$$

$$\frac{d\theta}{\theta} = \frac{-\, h\pi D}{Gc_p}\, dL\,.$$

Now

$$Re = \frac{4G}{\pi D\mu}\,,\ Nu = \frac{hD}{\lambda}\,, \text{ and } Pr = \frac{c_p\mu}{\lambda}\,.$$

Therefore,

$$\frac{d\theta}{\theta} = \frac{-\, 4Nu}{Pr\ Re}\ \frac{dL}{D}\,, \text{ the solution to which is:}$$

$$\frac{t_{g1} - t_s}{t_{g2} - t_s} = \exp \frac{4Nu}{Pr\ Re}\ \frac{L}{D}\,. \qquad (20)$$

For developed turbulent flow in a circular pipe the relationship between Nu and Re is given by McAdams[5] as:

$$Nu = 0{\cdot}023 Pr^{0{\cdot}4}\ Re^{0{\cdot}8}\,, \qquad (21)$$

so that:

$$\frac{t_{g1} - t_s}{t_{g2} - t_s} = \exp\left(0{\cdot}092 Pr^{-0{\cdot}6}\ Re^{-0{\cdot}2}\ \frac{L}{D}\right).$$

For air

$$Pr = 0{\cdot}71, \text{ and:}$$

$$\frac{t_{g1} - t_s}{t_{g2} - t_s} = \exp\left(0{\cdot}113 Re^{-0{\cdot}2}\ \frac{L}{D}\right). \qquad (22)$$

For the gas-heated blades when $t = 0$ deg C this suggests a relationship of the form:

$$\frac{t_{g1}}{t_{g2}} = \exp\left(K\ Re_g^{-m}\ \frac{L_g}{D_g}\right). \qquad (24)$$

APPENDIX IV

The Conduction Factor

Imagine a strip of metal of conductivity λ_m, as shown in Fig. 21, having unit width and uniform thickness δ, one side of which is subject to icing conditions and is anti-iced by heat applied at one side only. The heat is dissipated by convection and evaporation and in raising the temperature of the impinging water up to the surface temperature, t_s. If the water is assumed to be at the local effective air temperature, t_1'', then the total heat dissipation per unit area is proportional to $t_s - t_1''$, and may be represented by an effective heat-transfer coefficient h_a^1.

Consider then an element of length dx. Under equilibrium conditions the heat dissipated by the element must equal the heat conducted into it, so that:

$$h_a' (t_s - t_1'') \, dx = \lambda_m \frac{d^2 t_s}{dx^2} \delta \, . \qquad \ldots \ldots \ldots \ldots \ldots \quad (4.3)$$

Let $t_s - t_1'' = \phi$, then:

$$\frac{d^2\phi}{dx^2} = \frac{h_a'\phi}{\lambda_m \delta} \, .$$

Let l be the length of the strip and $\dfrac{h_a' l^2}{\lambda_m \delta} = \gamma^2$.

Then $$\frac{d^2\phi}{dx^2} = \left(\frac{\gamma}{l}\right)^2 \phi \, .$$

The solution to this equation is:

$$\phi = A \, e^{\gamma(x/l)} + B \, e^{-\gamma(x/l)} \, , \qquad \ldots \ldots \ldots \ldots \quad (4.4)$$

where A and B are constants.

At $x/l = 1 \cdot 0$ two conditions are satisfied; firstly there is no heat conduction, and secondly the surface temperature at this point, which is the minimum, is 0 deg C. From these conditions the values of the constants are found to be:

$$A = - \frac{t_1'' \gamma}{2 \, e} \text{ and } B = \frac{t_1''}{2 \, e^{-\gamma}}$$

so that

$$\phi = - \frac{t_1''}{2} \left\{ \exp \gamma \left(\frac{x}{l} - 1 \right) + \exp - \gamma \left(\frac{x}{l} - 1 \right) \right\}.$$

Let $l - x = y$, then:

$$\phi = - t_1'' \cosh \gamma \frac{y}{l} \, . \qquad \ldots \ldots \ldots \ldots \quad (4.5)$$

The total heat dissipated from the surface is given by:

$$H = l \int_0^1 \phi h_a' \, d\left(\frac{y}{l}\right)$$

$$= - l h_a' t_1'' \frac{\sinh \gamma}{\gamma} \, .$$

If the surface is maintained at a uniform temperature of 0 deg C, the total heat required is:

$$H = - lha't_1'' ,$$

so that the distribution efficiency is theoretically:

$$\eta'' = \frac{\gamma}{\sinh \gamma}$$

$$\eta'' \simeq \frac{1}{1 + (\gamma^2/3!)} \quad \ldots \ldots \ldots \ldots \ldots \ldots \ldots \quad (4.6)$$

In the wind-tunnel tests $t_1'' = t_1' \simeq t_w$ so that the assumption regarding water temperature is correct. In an engine the water temperature will be lower than t_1'' but since the heat required to raise the water temperature is only a small proportion of the total, the latter will still be approximately proportional to $(0 - t_1'')$ and the above reasoning will apply.

In the tunnel, therefore:

$$h_a' = \frac{H_e}{S_a(0 - t_1'')}$$

but in the engine:

$$h_a' \simeq \frac{H_e}{S_a(0 - t_1'')} \quad \ldots \ldots \ldots \ldots \ldots \ldots \ldots \quad (4.7)$$

APPENDIX V

Calculation of Requirements for Anti-Icing a Row of Inlet Guide Vanes

In the following worked example the requirements of mass flow and pressure for anti-icing a row of inlet guide vanes from a compressor bleed are calculated for a hypothetical engine at one particular flight condition. Minimum drag speed at 20,000 ft with 1·0 gm/m³ water content has been chosen as this probably represents one of the most difficult conditions for the gas-heated blade. However, to ensure that complete protection is afforded over the whole range of conditions likely to be encountered, many such calculations would have to be made.

The blade dimensions and basic engine data are represented in Fig. 22. The engine has forty steel inlet guide vanes of the Z_1-type heated by a compressor bleed.

The critical heat quantity:

$$H_c = h_m\left\{(0 - t_1') + 0{\cdot}622\frac{L_s}{c_p}\left(\frac{4{\cdot}58 - e_1}{p_1}\right)\right\} S_a + \eta_c V_1 n S_p(0 - t_w) \qquad .. \quad (15)$$

to find h_m:

$$Re_1 = \frac{V_1 c \rho_m}{\mu} = \frac{337 \times 0{\cdot}208 \times 0{\cdot}0423}{1{\cdot}08 \times 10^{-5}}$$

$$= 2{\cdot}75 \times 10^5.$$

Then from the graph of Nu vs. Re, Fig. 14a, $Nu = 420$.

Now
$$h_m = \frac{Nu\lambda}{c} = \frac{420 \times 3{\cdot}61 \times 10^{-6}}{0{\cdot}208}$$

$$= 7{\cdot}3 \times 10^{-3} \text{ CHU/ft}^2 \text{ sec deg C.}$$

In equation (15) t_1' is the temperature which the blade would assume in dry air, but in air partly saturated with water vapour[3], the corresponding temperature, because of evaporation from the surface is given by:

$$t_1'' = t_1' - 0{\cdot}622\frac{L_s}{c_p}\left(\frac{e_1'' - e_1}{p_1}\right) \text{ where } e_1'' = \text{saturation vapour pressure corresponding to } t_1''.$$

As e_1'' is a function of t_1'', t_1'' may only be found by trial and error; for the case considered $t_1'' = -18{\cdot}1$ deg C.

The projected area, S_p, with 0 deg C incidence is scaled from the model blade.

Thus
$$S_p = 1{\cdot}31 \times \frac{7{\cdot}5}{3{\cdot}0} \times \frac{2{\cdot}5}{1{\cdot}3} = 6{\cdot}3 \text{ in}^2\text{/blade.}$$

Assuming a water content, $n = 1{\cdot}0$ gm/m³ $= 6{\cdot}2 \times 10^{-5}$ lb/ft³, an efficiency of catch, $\eta_c = 1{\cdot}0$ and that t_w remains equal to t_0:

$$H_c = 7{\cdot}3 \times 10^{-3}\left\{18{\cdot}1 + 0{\cdot}622\frac{606}{0{\cdot}24}\left(\frac{4{\cdot}58 - 1{\cdot}3}{368}\right)\right\}\frac{40 \times 2 \times 7{\cdot}5 \times 2{\cdot}5}{144}$$

$$+ 1{\cdot}0 \times 337 \times 6{\cdot}2 \times 10^{-5} \times \frac{40 \times 6{\cdot}3}{144} \times 24{\cdot}6$$

$$= 3{\cdot}34 \text{ CHU/sec/blade row.}$$

Determination of Re_g and G_g

$$f(Re_g) = Re_g\left[1 - \exp\left(-K\,Re_g^{-m}\frac{L_g}{D_g}\right)\right] = \frac{4H_c}{c_{pg}\mu_g Z_g t_{g\,1}\eta''} \quad .. \quad .. \quad .. \quad .. \quad (34)$$

where

$$\eta'' = \frac{1}{1 + \{h_a'(l/c)^2\,c^2/6\,\Sigma\lambda_m\delta\}} \quad .. \quad .. \quad (32)$$

Now

$$h_a' = \frac{H_c}{S_a(0 - t_1'')} = \frac{3{\cdot}34}{10{\cdot}92 \times 18{\cdot}1}$$

$$= 1{\cdot}69 \times 10^{-2}\ \text{CHU/ft}^2\ \text{sec deg C.}$$

Assuming the blade material is steel, $\lambda_m = 3{\cdot}23 \times 10^{-3}$ CHU/ft sec deg C and thickness, δ, is 0·042 in,

then

$$\eta'' = 1 + \frac{1}{\{1{\cdot}69 \times 10^{-2}(0{\cdot}4)^2 \times 0{\cdot}208^2/6 \times 3{\cdot}32 \times 10^{-3}\} \times 0{\cdot}042/12}$$

$$= 0{\cdot}367.$$

With a compressor delivery temperature of 148 deg C and allowing a 10 deg C drop in the ducting, $t_{g\,1} = 138$ deg C.

and

$$f(Re_g) = \frac{4 \times (3{\cdot}34/40)}{0{\cdot}24 \times 1{\cdot}16 \times 10^{-5} \times 0{\cdot}105 \times 138 \times 0{\cdot}367}$$

$$= 2{\cdot}26 \times 10^4.$$

Hence, when $K = 0{\cdot}50$ and $m = 0{\cdot}36$, *i.e.*, for a Z_1 blade:

$Re_g = 2{\cdot}67 \times 10^4$ (found by plotting Re_g versus $f(Re_g)$) .

Now

$$Re_g = \frac{4G_g}{Z_g\mu_g}. \quad .. \quad .. \quad .. \quad .. \quad .. \quad .. \quad .. \quad .. \quad (19)$$

Therefore

$$G_g = \frac{2{\cdot}67 \times 10^4 \times 0{\cdot}105 \times 1{\cdot}16 \times 10^{-5}}{4}$$

$$= 8{\cdot}15 \times 10^{-3}\ \text{lb/sec/blade.}$$

Total flow required $= 40 \times 8{\cdot}15 \times 10^{-3} = 0{\cdot}326$ lb/sec.

The compressor mass flow, G_a, is 52 lb/sec. Therefore, this represents a compressor bleed of $(0{\cdot}326/52) \times 100 = 0{\cdot}625$ per cent.

Determination of pressure drop

$$p_{g\,1}^2 - p_{g\,2}^2 = \frac{Re_g^2 R_g T_{g\,m}\mu_g^2}{gD_g^2}\left(f_m\frac{4L_g}{D_g} + B\right) \quad .. \quad .. \quad .. \quad .. \quad .. \quad (36)$$

where

$$f_m = 0{\cdot}079\ Re_g^{-02{\cdot}5} \quad .. \quad .. \quad .. \quad .. \quad .. \quad .. \quad .. \quad (38)$$

$$= 0{\cdot}079 \times (2{\cdot}67 \times 10^4)^{0{\cdot}25}$$

$$= 6{\cdot}19 \times 10^{-3}$$

and
$$T_{g\,m} = t_{g\,1}\left[\frac{1 + \exp\{-K\,Re_g^{-m}\,(L_g/D_g)\}}{2}\right] + 273 \quad .. \quad .. \quad .. \quad (37)$$

$$= 138\left[\frac{1 + \exp\{-0{\cdot}50\,(2{\cdot}67 \times 10^4)^{-0{\cdot}36} \times 147\}}{2}\right] + 273$$

$$= 352{\cdot}7 \text{ deg C abs.}$$

$$p_{g\,1}{}^2 - p_{g\,2}{}^2 = \frac{(2{\cdot}67 \times 10^4)^2 \times 96 \times 352{\cdot}7 \times (1{\cdot}16 \times 10^{-5})^2}{32{\cdot}2 \times (1{\cdot}5 \times 10^{-2})^2}\,(6{\cdot}19 \times 10^{-3} \times 4 \times 147 + 5{\cdot}7)$$

$$= 4{\cdot}47 \times 10^5\,(3{\cdot}64 + 5{\cdot}7)\ (\text{lb/ft}^2)^2$$

$$= 2{\cdot}01 \times 10^2\ (\text{lb/in.}^2)^2.$$

Assuming a compressor delivery pressure of 30·8 lb/in.² and a loss of 2·8 lb/in.² in the ducting, $p_{g\,1} = 28{\cdot}0$ lb/in.².

Therefore
$$p_{g\,2}{}^2 = 784 - 201,$$

$$p_{g\,2} = 24{\cdot}1 \text{ lb/in.}^2.$$

TABLE 1

Maximum Instantaneous Icing Conditions

Altitude $a \times 10^{-3}$ (ft)	Air temperature t (deg C)	Concentration n (gm/m³)	Droplet size d microns
18 to 20	0	5·0	25
22 to 25	— 10	4·0	25
25 to 30	— 20	3·0	25
20 to 30	— 30	2·0	20
20 to 30	— 40	0·5	15

TABLE 2

Empirical Heat-Transfer Factors

Blade	Z_1	Z_2	Z_3	$U_{T.E.}$	E	I
K	0·500	0·568	1·432	5·36	20·4	0·284
m	0·36	0·43	0·50	0·61	0·72	0·25

TABLE 3

Esitmated Values of the Equivalent Length

Blade	Z_1	Z_2	Z_3	$U_{T.E.}$	$U_{L.E.}$	E	I	II_a	II_b
l ft	0·0435	0·0352	0·0490	0·0785	0·1113	0·060	0·0795	0·152	0·165
l/c	0·40	0·32	0·45	0·72	1·04	0·55	0·73	1·40	1·52

TABLE 4

The Pressure-Loss Components

Blade	Z_1	Z_2	Z_3	$U_{T.E.}$	E	I
$\frac{p_{g\,m}\Delta p_g}{G_g^2}\ \frac{2_g}{R_g T_{g\,m}} \times 10^{-3}$ .... (in.$^{-4}$)	40	24	48	9·8	3·2	1·35
$\frac{p_{g\,m}\Delta p_g}{G_g^2}\ \frac{2_g}{R_g T_{g\,m}} A_g^2$	9·3	13·8	27·6	11·7	6·7	6·8
$f_m \frac{4L_g}{D_g}$	3·6	3·2	3·5	2·0	1·2	0·9
$B = \alpha + \beta\left(\frac{A_g}{A_i}\right)^2$	5·7	10·6	24·1	9·7	5·5	5·9
β	3·6	3·6	3·6	3·6	3·6	3·6
$\beta\left(\frac{A_g}{A_i}\right)^2$	1·1	2·7	2·7	4·9	2·4	5·9
α	4·6	7·9	21·4	4·8	3·1	0

TABLE 5

The Rate of Cooling of a Water Droplet

($t = -20$ deg C, $d = 20$)

t_{W1} deg C	50	40	30	20	10	0	−10	−15	−19	−19·5	−19·8
t_{W2} deg C	40	30	20	10	0	−10	−15	−19·5	−19·5	−19·8	−19·9
$\lambda \times 10^6$ CHU/s ft deg C	4·4	4·3	4·2	4·1	4·0	3·9	3·8	3·75	3·7	3·7	3·7
$1 + X$	2·79	2·26	1·870	1·586	1·391	1·261	1·190	1·157	1·139	1·142	1·138
$\Delta\tau = 10^3 s$	0·280	0·419	0·636	0·980	1·792	3·14	3·43	8·31	3·67	4·84	3·68
$\tau \times 10^3 s$	0·280	0·699	1·335	2·315	4·107	7·25	10·68	18·99	21·66	26·50	30·18

TABLE 6

An Estimate of the Ice Formed under the Trailing-Edge Icing Condition

Blade incidence, i	Stator + 10 deg	Stator 0 deg	Stator − 10 deg	I.G.V. 0 deg
Value of t_1 with no heat applied and ice just forming at T.E. deg C	− 1·5	− 2·0	− 0·9	− 1·8
External Reynolds number $Re_1 \times 10^5$	2·55	2·55	2·55	1·75
Equivalent heat-transfer coefficient $h_a' \times 10^2$ CHU/ft² s deg C	2·44	2·44	2·44	1·79
Heat dissipated $H_e/S_a \times 10^2$ CHU/ft² s	3·66	4·88	2·20	3·22
Equivalent percentage of water catch x per cent	9·1	11·6	11·6	11·1

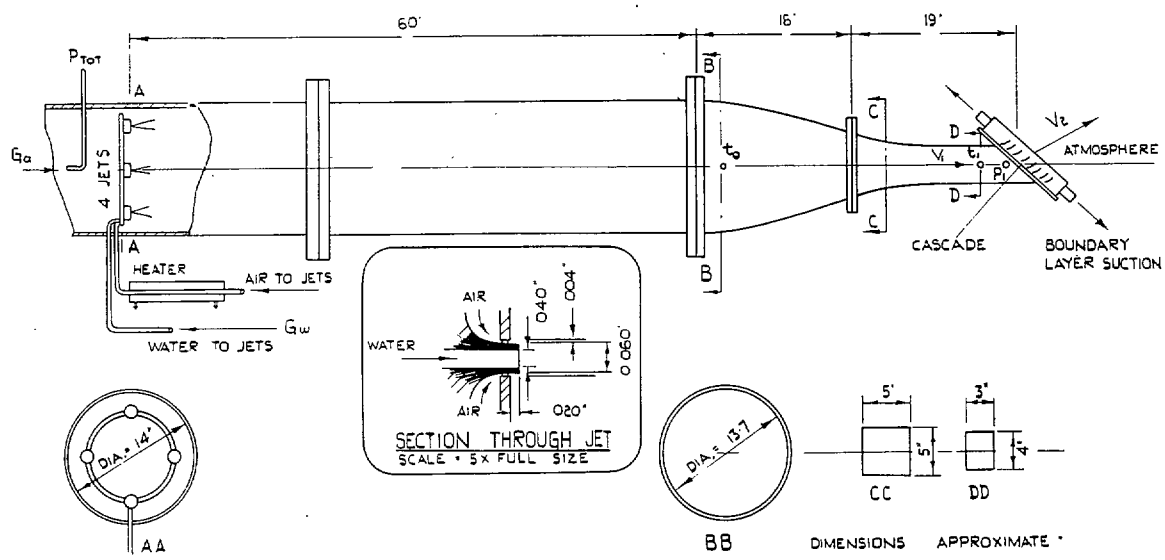

FIG. 1. The icing tunnel.

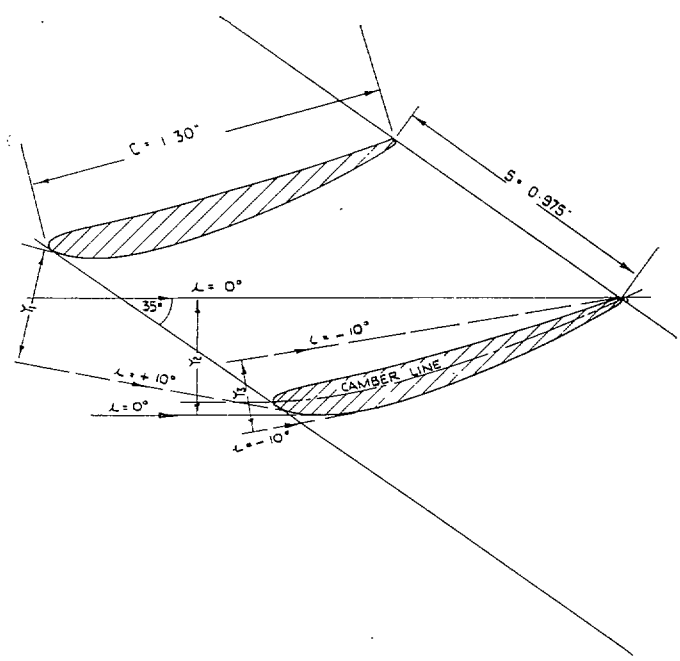

INCIDENCE α	Y - IN.	PROJECTED AREA YL - IN.^{2}
+10°	0·412	1·24
0°	0·437	1·31
−10°	0·232	0·76

FIG. 2. Area of catch.

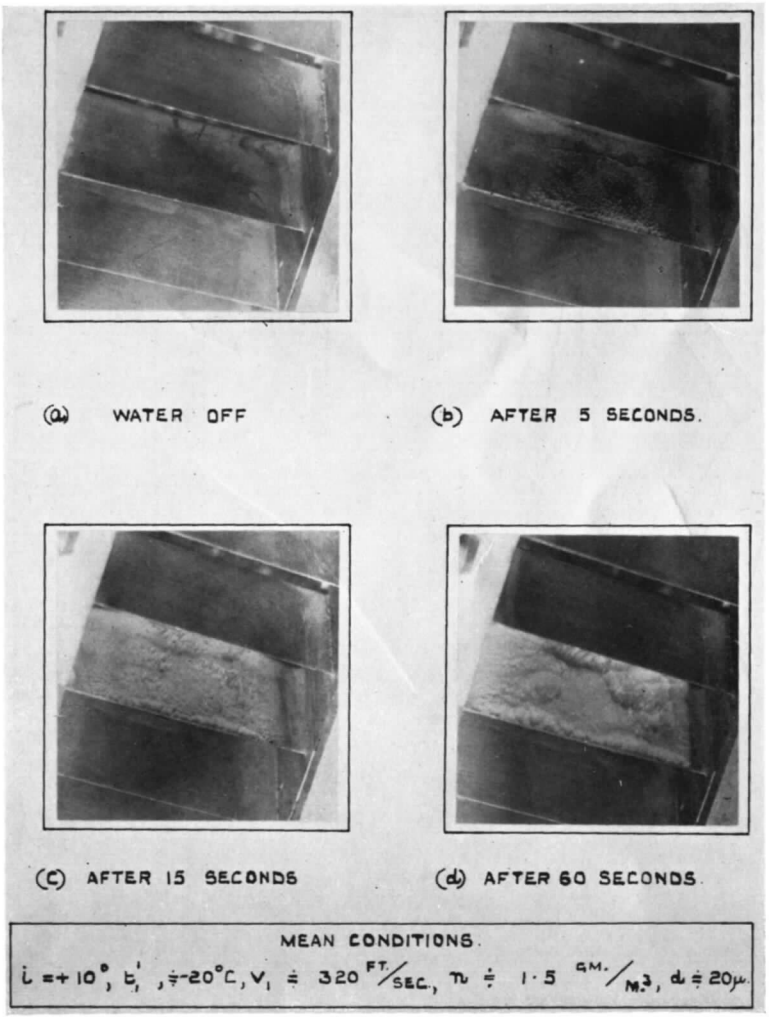

FIG. 3. Icing of a cascade of stator blades (No heat applied).

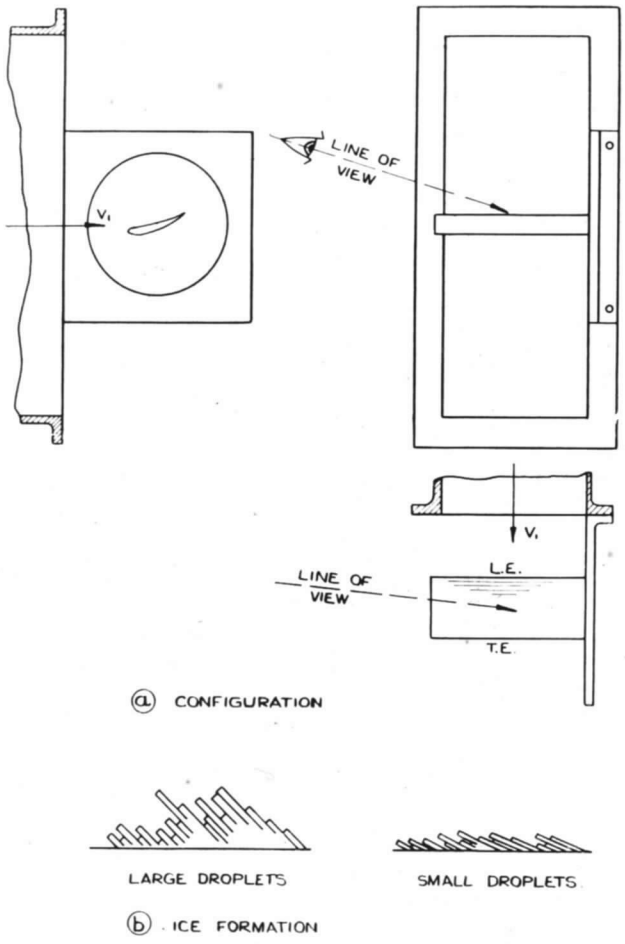

FIG. 4. The isolated compressor blade.

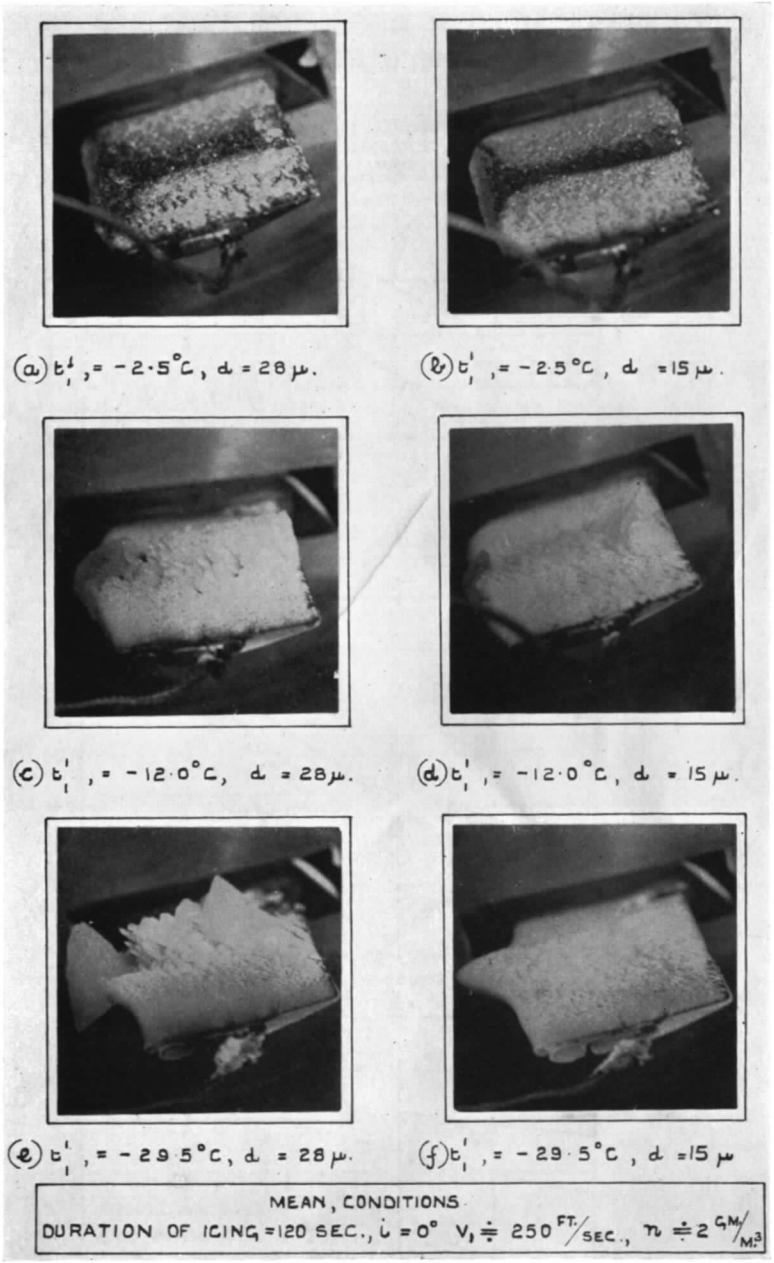

FIG. 5. Icing of an isolated compressor blade (No heat applied).

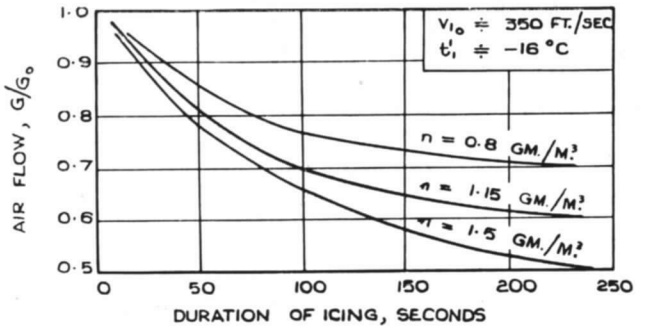

(a) EFFECT OF WATER CONCENTRATION

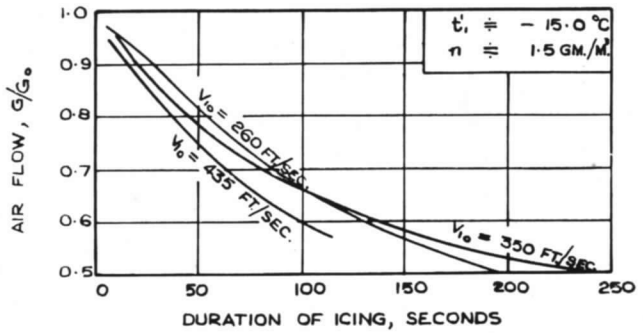

(b) EFFECT OF INITIAL AIR VELOCITY

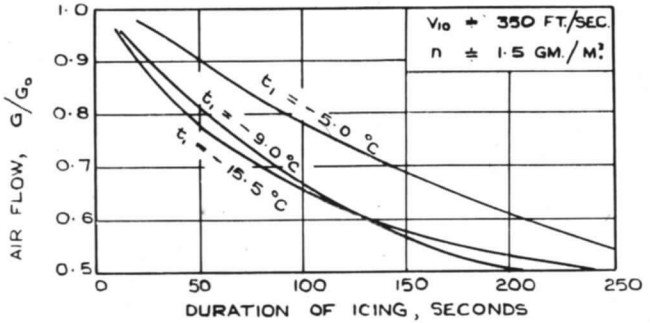

(c) EFFECT OF AIR TEMPERATURE

FIG. 6. Effect of ice accretion on the mass flow through an unheated stator cascade.

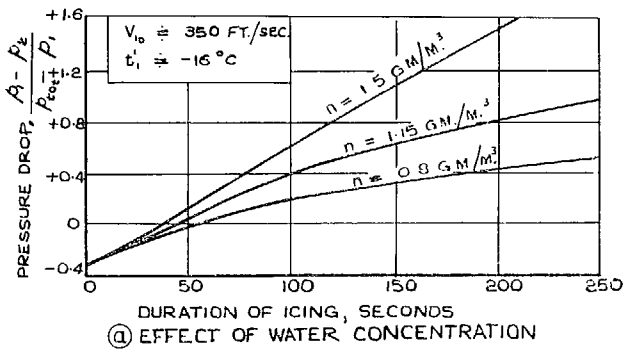

ⓐ EFFECT OF WATER CONCENTRATION

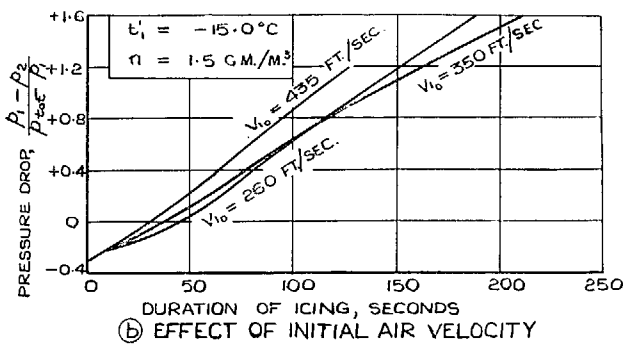

ⓑ EFFECT OF INITIAL AIR VELOCITY

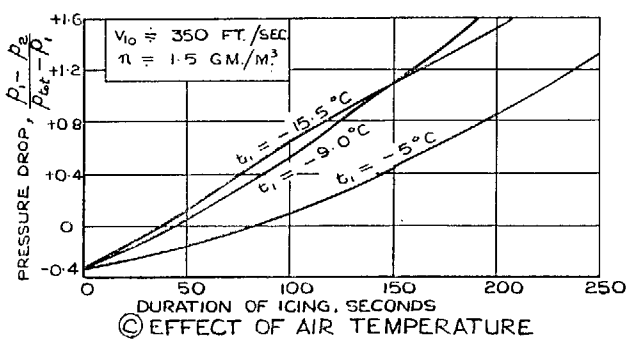

ⓒ EFFECT OF AIR TEMPERATURE

FIG. 7. Effect of ice accretion on the pressure drop across an unheated stator cascade.

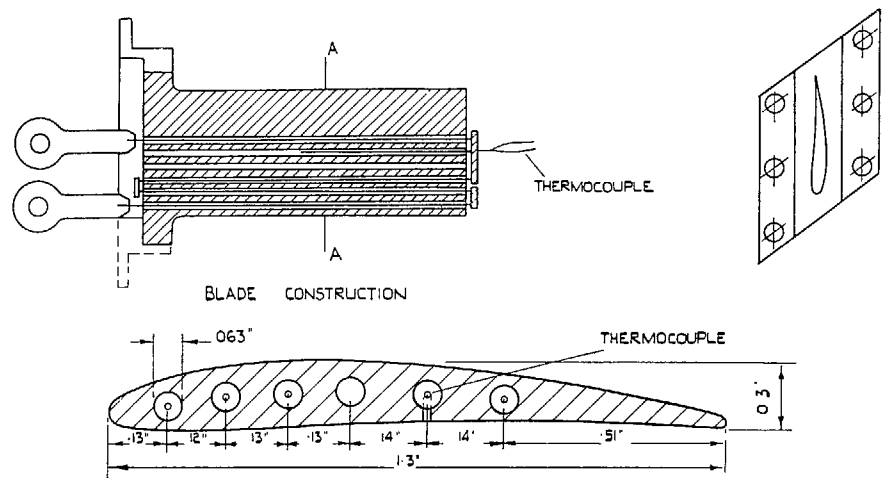

FIG. 8. The electrically heated blade.

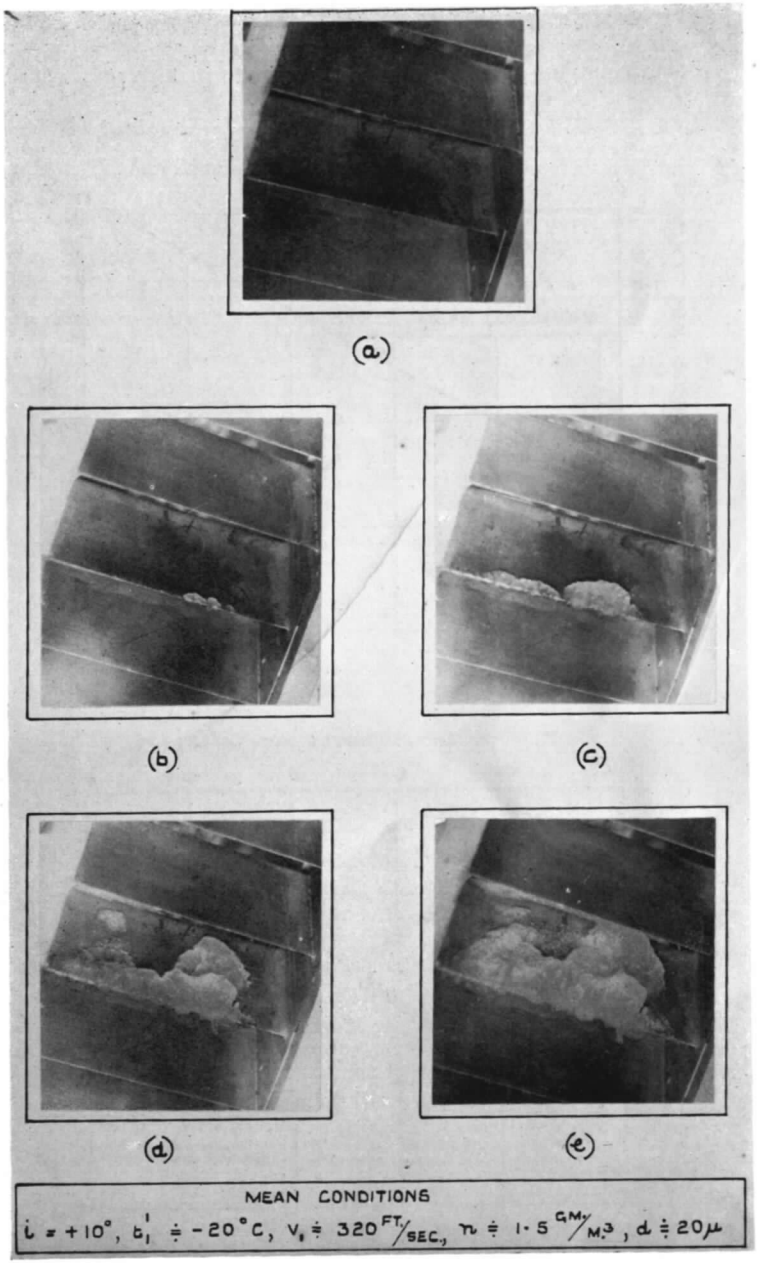

FIG. 9. Icing of a cascade of stator blades (Progressive reduction of heat applied).

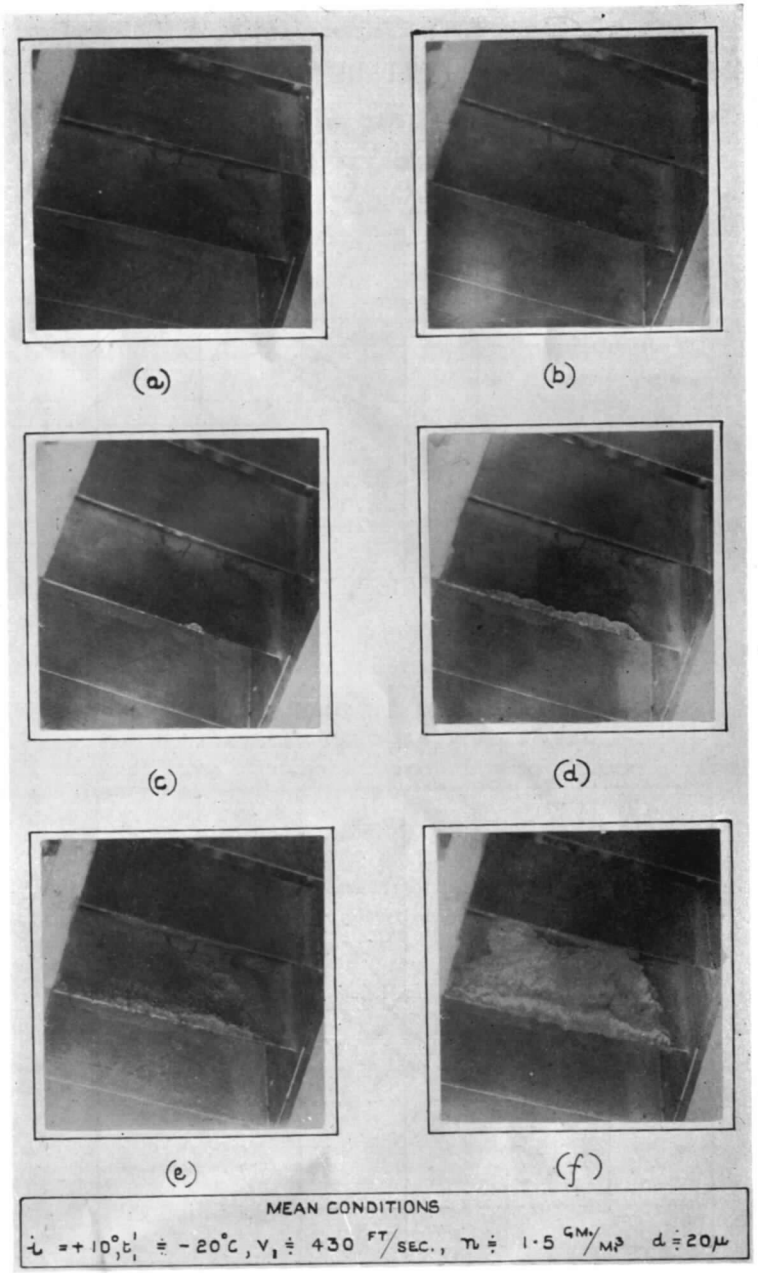

FIG. 10. Icing of a cascade of stator blades (Progressive reduction of heat applied).

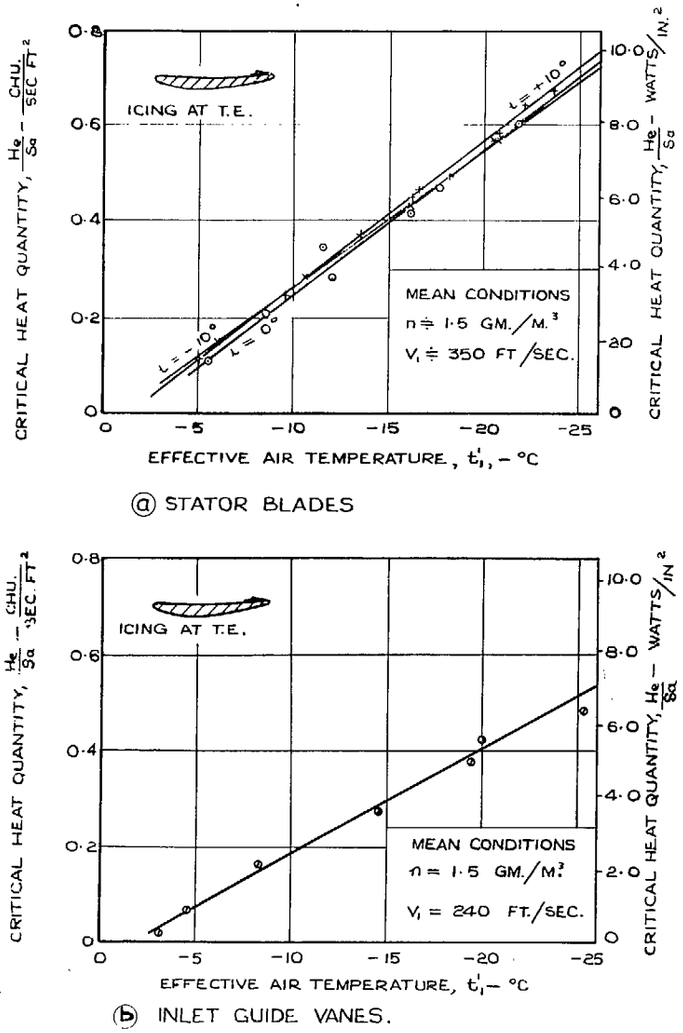

(a) STATOR BLADES

(b) INLET GUIDE VANES.

FIG. 11. Variation of critical heat quantity with air temperature.

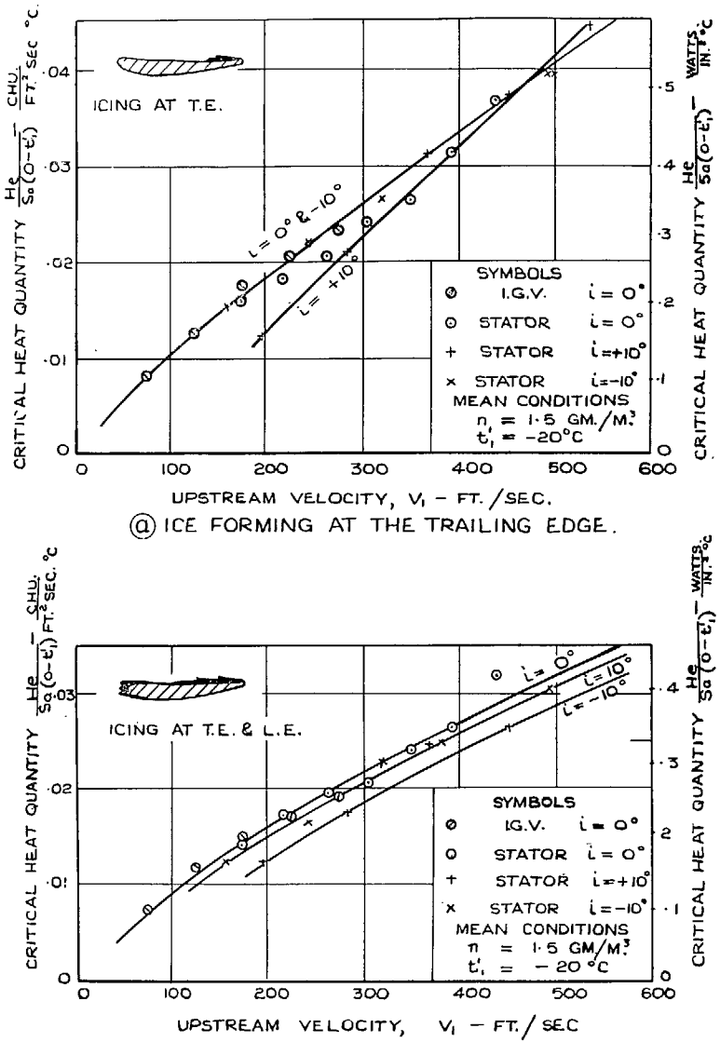

(a) ICE FORMING AT THE TRAILING EDGE.

(b) ICE FORMING AT THE TRAILING & LEADING EDGES.

FIG. 12. Variation of critical heat quantity with air velocity.

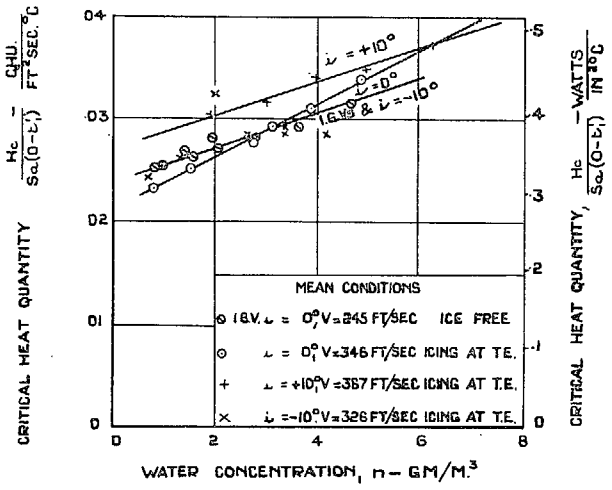

a.) VARIATION OF CRITICAL HEAT QUANTITY WITH WATER CONCENTRATION.

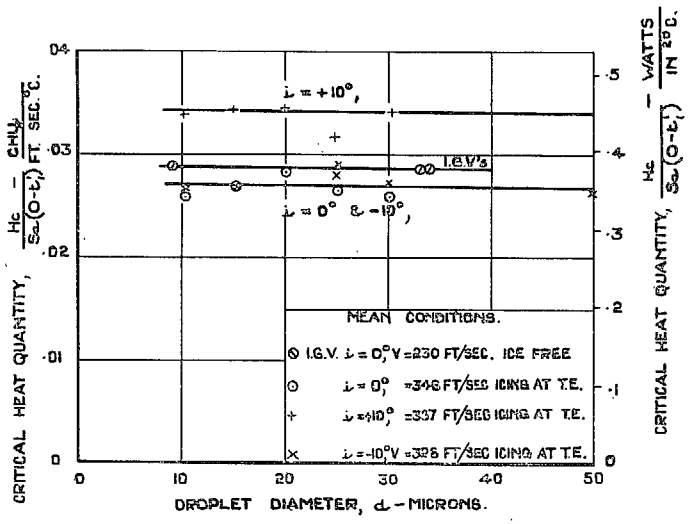

b.) VARIATION OF CRITICAL HEAT QUANTITY WITH DROPLET SIZE.

FIG. 13. Variation of critical heat quantity with water concentration and droplet size.

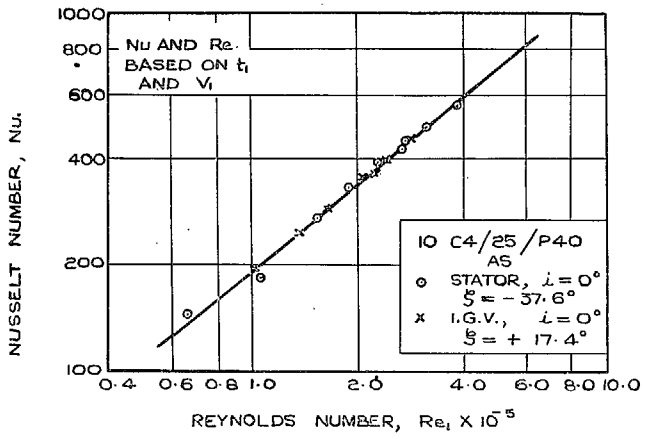

ⓐ EXPERIMENTAL HEAT TRANSFER CHARACTERISTICS

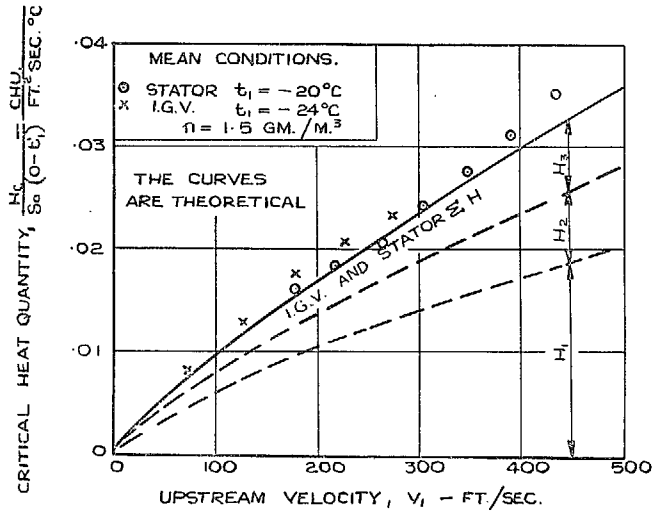

ⓑ COMPARISON BETWEEN TEST AND THEORY.

FIG. 14. A theoretical estimate of the critical heat quantity.

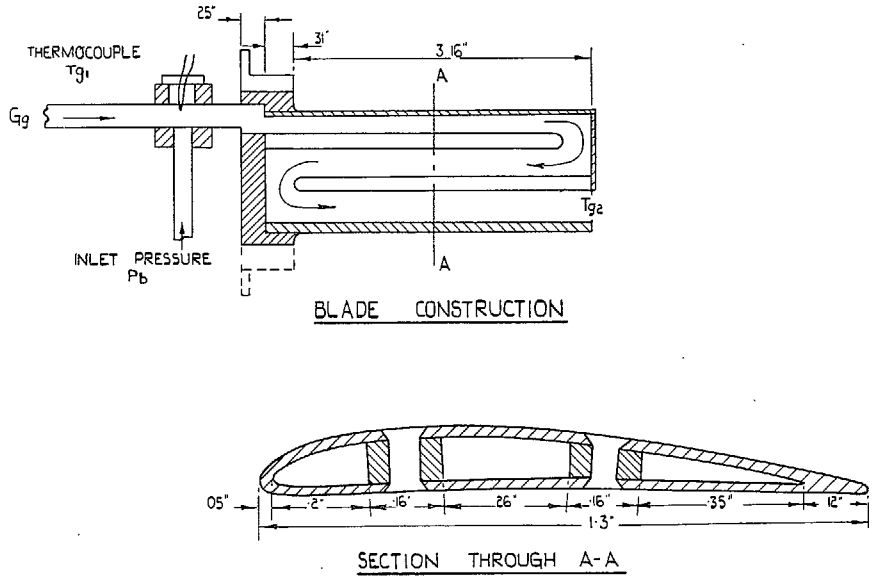

FIG. 15. A gas-heated blade with Z-flow.

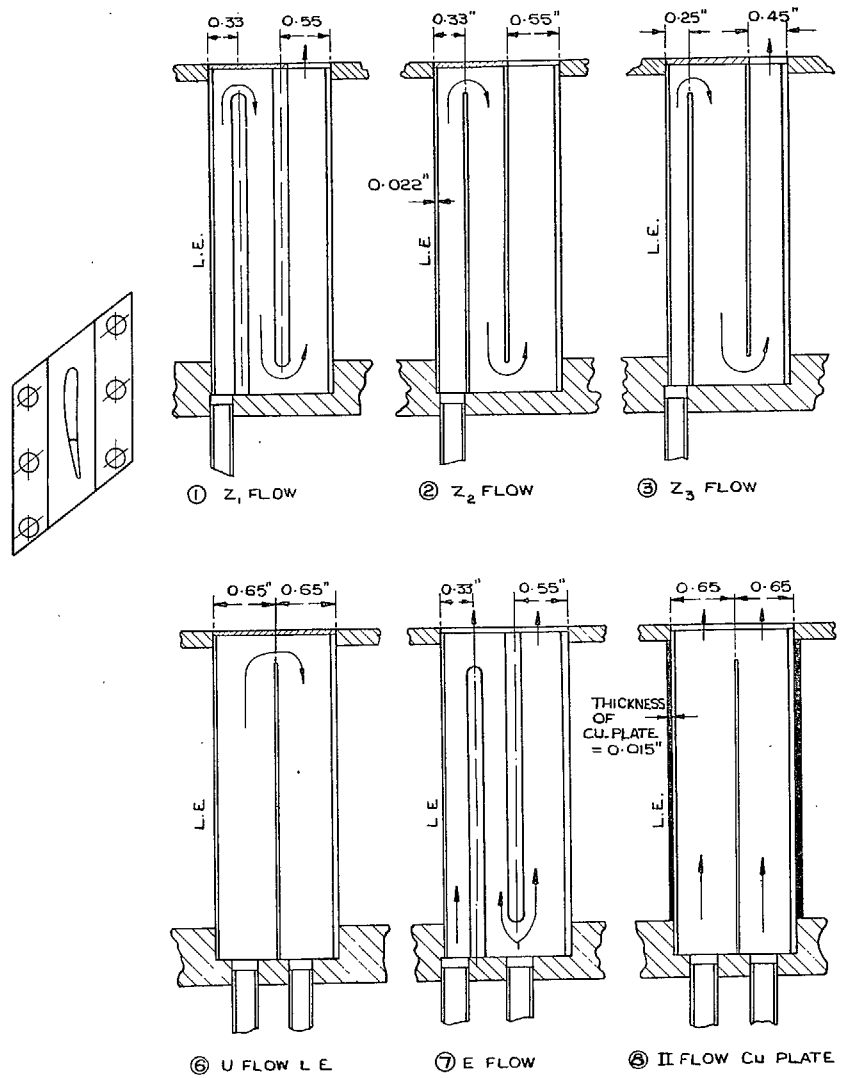

FIG. 16. The gas-heated blades.

TYPE OF BLADE		INTERNAL SURFACE AREA – S_g FT.^{2}	INTERNAL PERIMETER Z_g FT.	CROSS SECTIONAL AREA – A_g FT.^{2}	HYDRAULIC DIAMETER $D_g = \frac{4A_g}{Z_g}$ FT.	LENGTH / DIAMETER L_g/D_g
① AND ④	1		4.23×10^{-2}	0.80×10^{-4}	7.57×10^{-3}	
	2		5.86 "	1.59 "	10.84 "	
Z_1	3		6.25 "	0.78 "	4.99 "	
(L_g=0.885 FT.)	m	4.83×10^{-2}	5.45×10^{-2}	1.06×10^{-4}	7.80×10^{-3}	113
②	1.		5.58 "	1.29 "	9.24 "	
	2.		7.91 "	2.23 "	11.28 "	
Z_2	3.		7.16 "	1.01 "	5.64 "	
(L_g= 0 885 FT.)	m.	5.99×10^{-2}	6.88×10^{-2}	1.51×10^{-4}	8.72×10^{-3}	101
③	1.		4.25 "	0.82 "	7.72 "	
	2.		10.91 "	3.05 "	11.18 "	
Z_3	3		5.5 "	0 66 "	4.80 "	
(L_g=0.885FT)	m	5.99×10^{-2}	6.92×10^{-2}	1.51×10^{-4}	7.90×10^{-3}	112
⑤ AND ⑥	1		11.0 "	3.09 "	12 36 "	
	2		8.92 "	1.39 "	6 23 "	
U	m.	5.80×10^{-2}	9.96×10^{-2}	2.24×10^{-4}	9.30×10^{-3}	63
⑦ E (L_g=0.292 FT)		4.83×10^{-2}	16.36×10^{-2}	3.16×10^{-4}	7.73×10^{-3}	38
⑧ I (L_g= 0.292 FT)		5.57×10^{-2}	19.1×10^{-2}	4.91×10^{-4}	10.29×10^{-3}	28
⑨ AND ⑩ II (L_g= 0.292 FT.)		5.80×10^{-2}	19.9×10^{-2}	4.48×10^{-4}	8.99×10^{-3}	32

FIG. 17. Internal dimensions of the gas-heated blades.

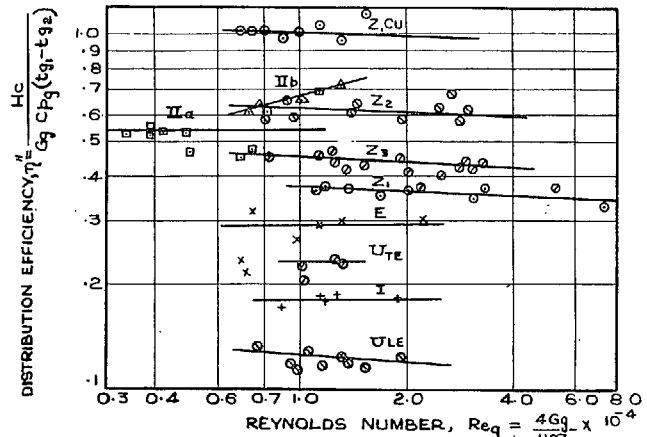

ⓐ DISTRIBUTION EFFICIENCY.

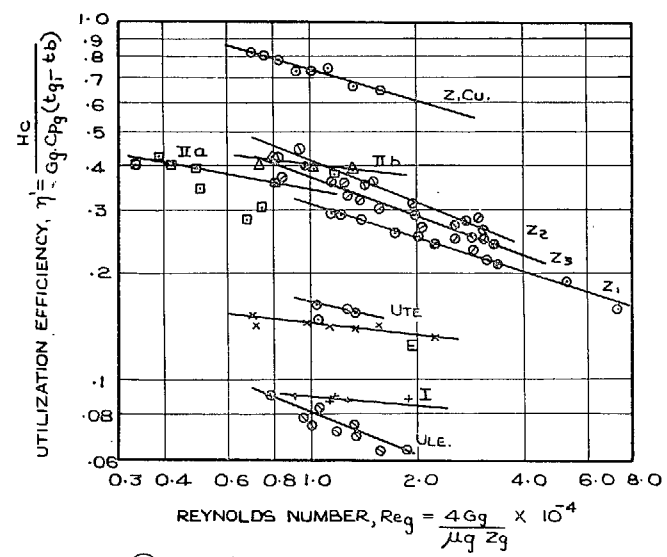

ⓑ UTILIZATION EFFICIENCY.

FIG. 18. Thermal efficiencies of the gas-heated blades.

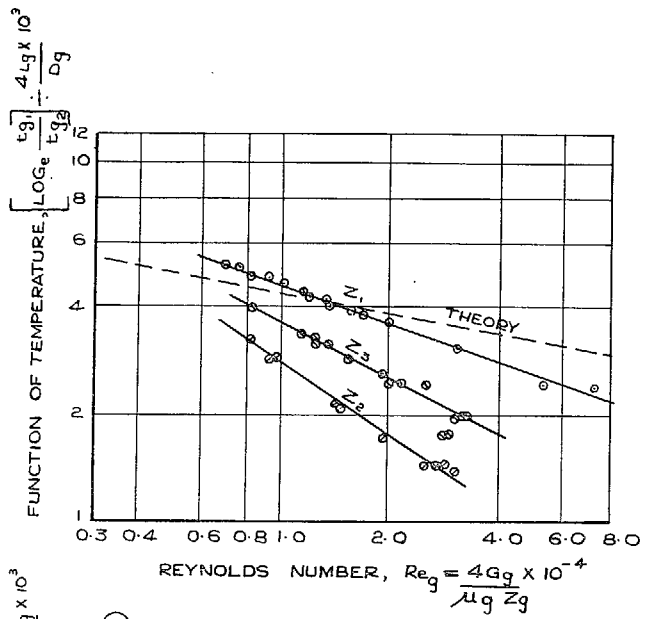

(a) Z – FLOW BLADES

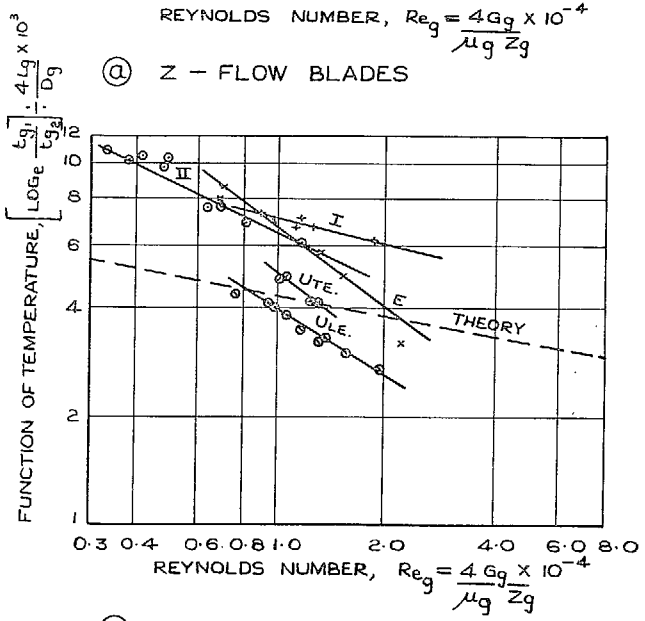

(b) OTHER BLADES.

FIG. 19. Temperature drop in the gas-heated blades.

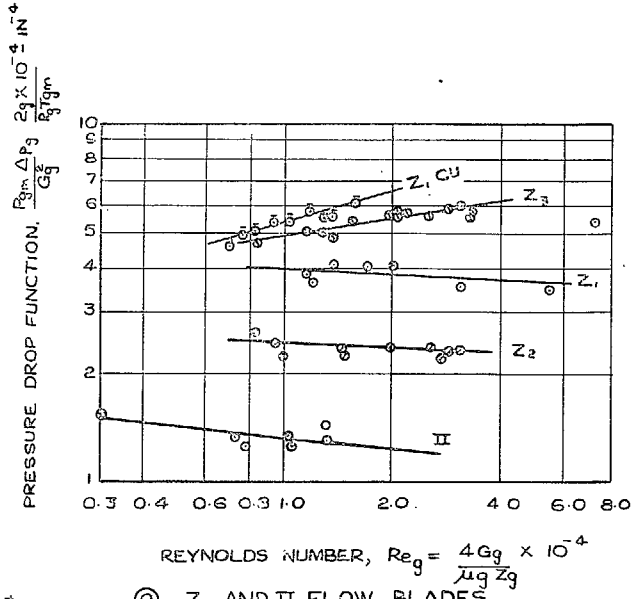

(a) Z AND II FLOW BLADES.

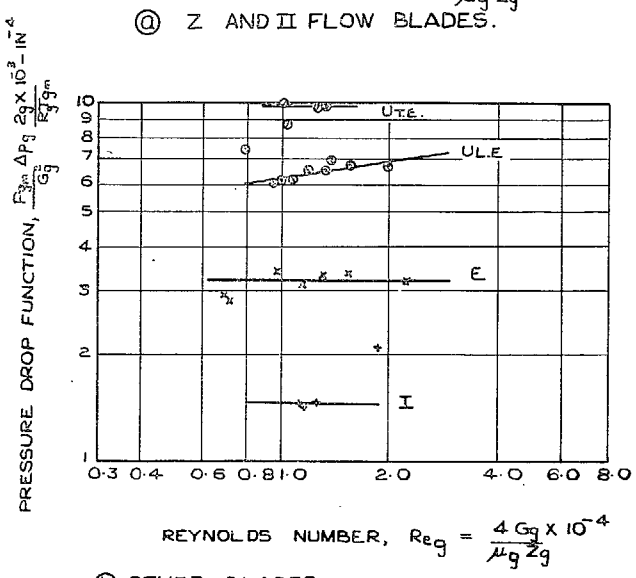

(b) OTHER BLADES.

FIG. 20. Pressure drop in the gas-heated blades.

Wt. 20 K7 7/57 F M. & S.

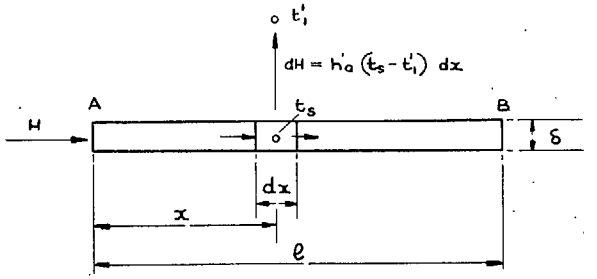

ⓐ DERIVATION OF γ

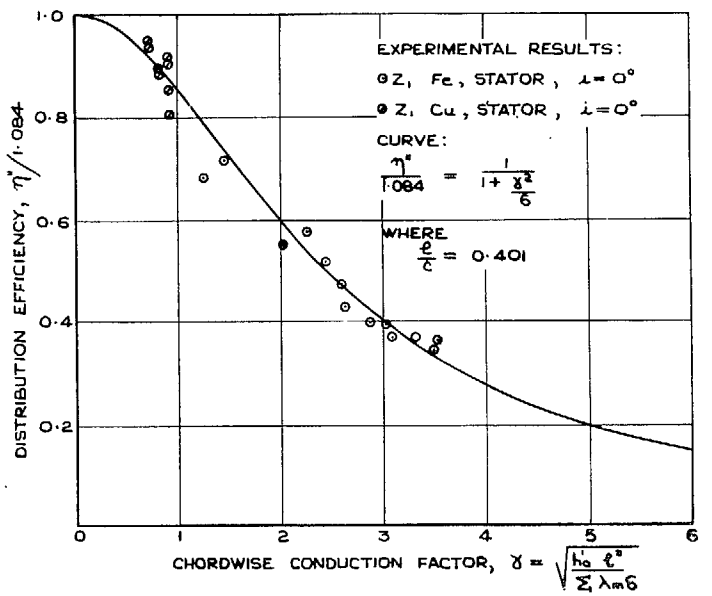

ⓑ RELATIONSHIP WITH η''

FIG. 21. The chrodwise conduction factor.

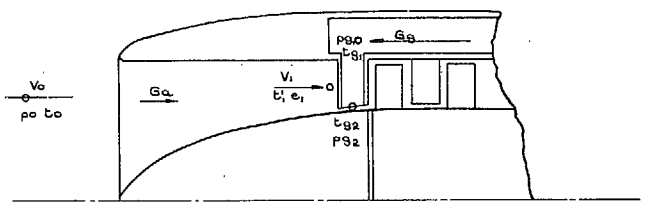

CONDITIONS AT ALTITUDE a = 20,000 FT - MINIMUM DRAG SPEED.

V_o = 451 FT/SEC	p_o = 6·75 LB/SQ.IN	G_a = 52 LB/SEC.
V_1 = 337 FT/SEC.	P_1 = 7·11 LB/SQ.IN	t'_1 = -16·1 °C.
p_{g_1} = 28·0 LB/SQ IN	t_{g_1} = 138 °C	t_o = -24·6° C

a.) AIR AND GAS CONDITIONS

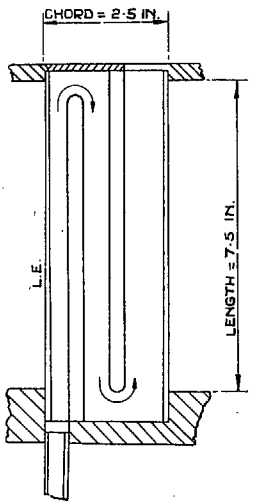

INTERNAL DIMENSIONS OF I.G.V.

DIMENSION	SYMBOL	UNITS	VALUE
LENGTH OF GAS PASSAGE	L_g	FT.	2·2
INTERNAL PERIMETER	Z_g	FT.	0·105
INTERNAL SURFACE AREA	S_g	FT.^{2}	0·231
CROSS SECTIONAL AREA	A_g	FT.^{2}	$3{\cdot}95\times10^{-4}$
HYDRAULIC DIA.	$D_g = \frac{4A_g}{Z_g}$	FT.	$1{\cdot}5\times10^{-2}$
LENGTH/DIAMETER	L_g/D_g	-	14·7

b.) BLADE DIMENSIONS

FIG. 22. Data for the worked example.

PRINTED IN GREAT BRITAIN

Publication of the Aeronautical Research Council

ANNUAL TECHNICAL REPORTS OF THE AERONAUTICAL RESEARCH COUNCIL (BOUND VOLUMES)

1939 Vol. I. Aerodynamics General, Performance, Airscrews, Engines. 50*s.* (52*s.*)
Vol. II. Stability and Control, Flutter and Vibration, Instruments, Structures, Seaplanes, etc. 63*s.* (65*s.*)

1940 Aero and Hydrodynamics, Aerofoils, Airscrews, Engines, Flutter, Icing, Stability and Control Structures, and a miscellaneous section. 50*s.* (52*s.*)

1941 Aero and Hydrodynamics, Aerofoils, Airscrews, Engines, Flutter, Stability and Control Structures. 63*s.* (65*s.*)

1942 Vol. I. Aero and Hydrodynamics, Aerofoils, Airscrews, Engines. 75*s.* (77*s.*)
Vol. II. Noise, Parachutes, Stability and Control, Structures, Vibration, Wind Tunnels. 47*s.* 6*d.* (49*s.* 6*d.*)

1943 Vol. I. Aerodynamics, Aerofoils, Airscrews. 80*s.* (82*s.*)
Vol. II. Engines, Flutter, Materials, Parachutes, Performance, Stability and Control, Structures. 90*s.* (92*s.* 9*d.*)

1944 Vol. I. Aero and Hydrodynamics, Aerofoils, Aircraft, Airscrews, Controls. 84*s.* (86*s.* 6*d.*)
Vol. II. Flutter and Vibration, Materials, Miscellaneous, Navigation, Parachutes, Performance, Plates and Panels, Stability, Structures, Test Equipment, Wind Tunnels. 84*s.* (86*s.* 6*d.*)

1945 Vol. I. Aero and Hydrodynamics, Aerofoils. 130*s.* (132*s.* 9*d.*)
Vol. II. Aircraft, Airscrews, Controls. 130*s.* (132*s.* 9*d.*)
Vol. III. Flutter and Vibration, Instruments, Miscellaneous, Parachutes, Plates and Panels, Propulsion. 130*s.* (132*s.* 6*d.*)
Vol. IV. Stability, Structures, Wind Tunnels, Wind Tunnel Technique. 130*s.* (132*s.* 6*d.*)

Annual Reports of the Aeronautical Research Council—

1937 2*s.* (2*s.* 2*d.*) 1938 1*s.* 6*d.* (1*s.* 8*d.*) 1939–48 3*s.* (3*s.* 5*d.*)

Index to all Reports and Memoranda published in the Annual Technical Reports, and separately—

April, 1950 - - - - R. & M. 2600 2*s.* 6*d.* (2*s.* 10*d.*)

Author Index to all Reports and Memoranda of the Aeronautical Research Council—

1909—January, 1954 R. & M. No. 2570 15*s.* (15*s.* 8*d.*)

Indexes to the Technical Reports of the Aeronautical Research Council—

December 1, 1936—June 30, 1939	R. & M. No. 1850	1*s.* 3*d.* (1*s.* 5*d.*)
July 1, 1939–June 30, 1945	R. & M. No. 1950	1*s.* (1*s.* 2*d.*)
July 1, 1945—June 30, 1946	R. & M. No. 2050	1*s.* (1*s.* 2*d.*)
July 1, 1946—December 31, 1946	R. & M. No. 2150	1*s.* 3*d.* (1*s.* 5*d.*)
January 1, 1947—June 30, 1947	R. & M. No. 2250	1*s.* 3*d.* (1*s.* 5*d.*)

Published Reports and Memoranda of the Aeronautical Research Council—

Between Nos. 2251–2349	R. & M. No. 2350	1*s.* 9*d.* (1*s.* 11*d.*)
Between Nos. 2351–2449	R. & M. No. 2450	2*s.* (2*s.* 2*d.*)
Between Nos. 2451–2549	R. & M. No. 2550	2*s.* 6*d.* (2*s.* 10*d.*)
Between Nos. 2551–2649	R. & M. No. 2650	2*s.* 6*d.* (2*s.* 10*d.*)
Between Nos. 2651–2749	R. & M. No. 2750	2*s.* 6*d.* (2*s.* 10*d.*)

Prices in brackets include postage

HER MAJESTY'S STATIONERY OFFICE

York House, Kingsway, London W.C.2; 423 Oxford Street, London W.1; 13a Castle Street, Edinburgh 2; 39 King Street, Manchester 2; 2 Edmund Street, Birmingham 3; 109 St. Mary Street, Cardiff; Tower Lane, Bristol, 1; 80 Chichester Street, Belfast, *or through any bookseller.*

S.O. Code No. 23-3041